Significance of Active Tension Compensation During S-lay Pipeline Installation

Master of Science Thesis

Teddy Andreas Simanjuntak

Technische Universiteit Delft

TU Delft

Significance of Active Tension Compensation During S-lay Pipeline Installation

Master of Science Thesis

by

Teddy Andreas Simanjuntak

to obtain the degree of Master of Science
at the Delft University of Technology,
to be defended publicly on Friday, December 22nd, 2017 at 09:30 AM.

Student number:	4506391	
Email:	teddy.andreas.s@gmail.com	
Project duration:	January 18, 2017 – December 22, 2017	
Thesis committee:	Prof. Dr. Andrei V. Metrikine,	TU Delft: section Offshore Engineering, graduation professor
	Dr. Eng. François Gerspach,	Allseas Engineering, supervisor
	Dr. Hayo Hendrikse,	TU Delft: section Offshore Engineering, supervisor
	Dr. ir. Jan-Willem van Wingerden ,	TU Delft: Delft Center for Systems and Control, supervisor

This thesis is confidential and cannot be made public until December 31, 2022.

TU Delft

Allseas

The work presented in this report was performed at, and supported by Allseas Engineering. Their cooperation is hereby gratefully acknowledged.

Acknowledgements

The success of this graduation work would not have been possible without the guidance, insight and motivation of a long list of individuals who support me throughout the process. I especially would like to express my gratitude to:

My supervisor, François Gerspach for entrusting me with this interesting graduation topic, who consistently steered me in the right direction and gave me valuable feedback. Thanks for sharing a lot of data analysis knowledge with me, also for giving me a lot of advice concerning expressing my ideas in the report and presentations.

Professor Andrei Metrikine and Hayo Hendrikse for their valuable suggestions for the improvement of the research. Thanks for helping me to understand better the principles of hydromechanics and structural dynamics. Also, I would like to thank Jan-Willem van Wingerden for serving as supervisor who help me understand better about control system.

My colleagues from the Pipeline Engineering department and the other departments within Allseas Engineering, who created a friendly working atmosphere during my time at the company.

Indonesia Endowment Fund for Education (LPDP) who gave me the scholarship during the 2-year master program at TU Delft. Without their resource, I would not have this valuable experience.

Finally, I would like to thank my family, girlfriend and friends in the Netherlands and Indonesia who always supports me throughout the process.

Teddy Andreas Simanjuntak
Delft, December 2017

Abstract

During S-lay pipeline installation, tension fluctuations in the suspended pipeline are compensated by the tensioner system on the vessel. The goal of this thesis is to answer the questions: to what extent does the active tension compensation (ATC) influence the pipeline integrity during offshore installation. Secondly, which tensioner model should be used for pipelay analyses that can give accurate results? And lastly, what is the implication on the existing tensioner models (deadband and linear damping with velocity cap) that are currently used in pipelay analyses?

The pipelay operation is modelled in OrcaFlex with 7 case studies from shallow to deep water based on full-scale measurement data measured during offshore installation. For each case study, three types of measurement data are available: vessel motions, tensioner pay-out motion and pipeline top tension. Vessel motions and tensioner motion signals are used as inputs to the OrcaFlex model, whereas the measured tension signal is used for comparison with the output pipeline top tension for model validation.

It is observed that the ATC becomes more important in deeper water as the reduction in maximum von Mises strain in the sagbend and accumulated fatigue damage become more significant with increasing water depth. The maximum von Mises strain is found to be in between 0% and 2.2% lower from the model with uncompensated tension. Moreover, the reduction in accumulated fatigue damage is more significant as the allowable standby time increases between 3.2% and 19.5%.

Subsequently, different tensioner models are included in the simulation. The tensioner model computes the pay-out motion based on the pipeline top tension deviation from a set tension at each time step. The initial model with specified tensioner motion is then used as a benchmark for the other tensioner models. It is found that the existing tensioner models are not conservative as the maximum von Mises strain and accumulated fatigue damage are underestimated, with the exception of the accumulated fatigue damage in shallow water cases.

As an alternative to the existing tensioner model, a tensioner model with a PI controller is introduced to represent the PI controller of the tensioners systems on the vessel. This PI controller model scripted in Python is implemented as an external function to the OrcaFlex model.

The controller gains are tuned proportional to the logged controller gains from the vessel so that the tensioner model produces the pay-out signal similar to the measured pay-out. Based on the pipeline integrity check, the tensioner model with PI controller is valid and can be used for a more accurate investigation of the pipeline integrity in all cases.

Keywords: S-lay; active tension compensation; tensioner; offshore pipelines; pipeline integrity; sagbend; OrcaFlex, measurement; PI controller; Python.

Contents

List of Figures

List of Tables

1 Introduction

This chapter gives an introduction to the thesis topic, problem statement, final aim and the approach that is taken to accomplish the thesis goal.

1.1. Introduction to S-lay Pipeline Installation

Oil and gas field development involves laying kilometres of marine pipelines on the seabed to transport hydrocarbons. In this thesis, installation of marine pipelines from a surface vessel, a so-called *pipelay operation*, is considered. Technology in pipelay operation has been growing continuously, spurred by the need to install pipeline precisely along a desired subsea route while also preventing the pipeline from damage. There are several methods to install the marine pipeline, and the most common ways are S-lay, J-lay, and reeling.

Among the other pipelay techniques, the S-lay technique has the widest field of operation since it can be applied to almost all sizes of pipe in various water depths from shallow to deep water. S-lay technique is schematically illustrated in figure 1.1.

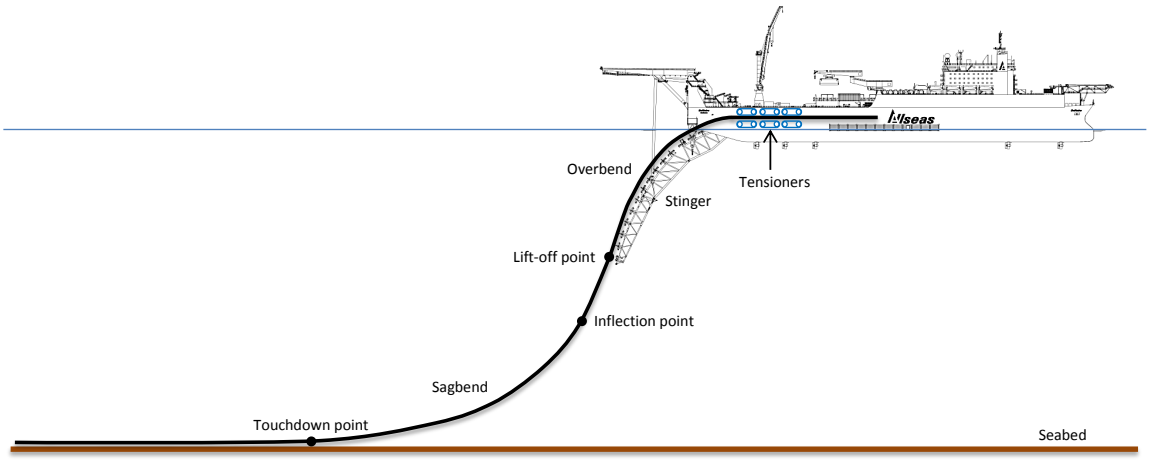

Figure 1.1: S-lay configuration

During offshore installation, the position of the pipelay vessel is maintained by either a dynamic positioning system or mooring lines. However, this system only compensates vessel motions due to low-frequency wave drift forces. Therefore, significant vessel motions caused by 1st order wave loads are still uncompensated. This type of vessel motions might jeopardize the suspended pipeline since they induce dynamic tension and dynamic bending moment in the pipeline. In order to reduce these dynamic effects, a pipelay vessel is equipped with tensioners, which compensates the tension fluctuation by paying out or hauling in the pipeline.

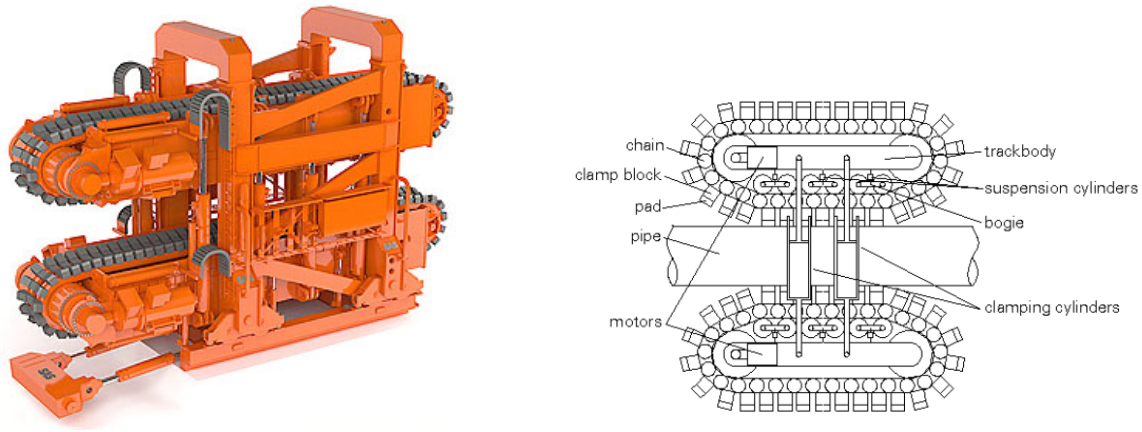

Figure 1.2: Tensioner used on pipelay vessel

As shown in figure 1.2, a tensioner consists of four tracks mounted in a frame, which grip the suspended pipeline and apply the tension force through friction. More importantly, the tensioners are also a tension controlling servo which makes pipelay operation possible in an environment where it is subjected to a number of disturbances. The servo system is a force control and the feedback signal is provided by load cells mounted on the structure carrying the tracks, which measure tension of the pipeline. Tensioners compensate the dynamic tension variations by paying-out and hauling-in pipeline. The influence of these tensioner motions is shown in the figure below.

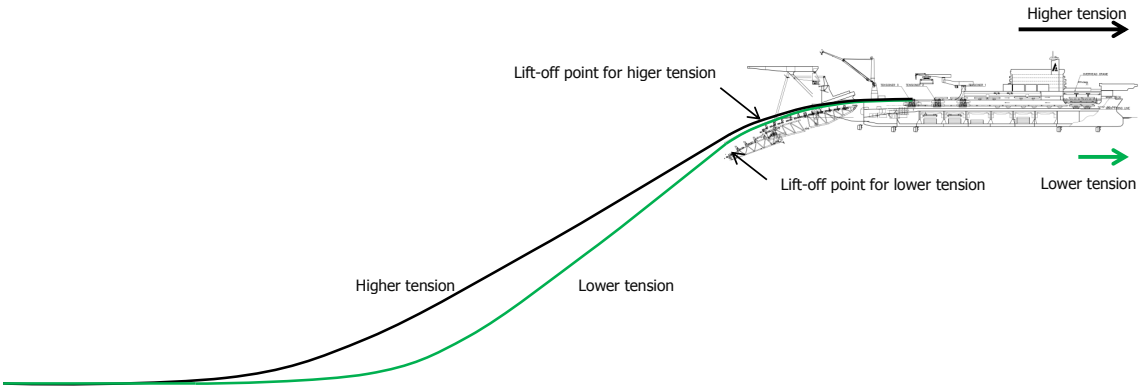

Figure 1.3: Schematic view of the change of pipeline curvature resulting from changes in tension

1.2. Research Goals

The goal of this thesis is to answer the questions: to what extent does the active tension compensation influence the pipeline integrity during offshore installation.; Secondly, which tensioner model should be used for pipelay analyses that can give accurate results?; And lastly, what is the implication on the existing tensioner models (deadband and linear damping with velocity cap) that are currently used in pipelay analyses?

Analysis and modelling for this thesis are limited only to normal pipelay operation, where there are no transition joints, no in-line structures, and the suspended pipeline is fully retained by tensioners on top of the vessel.

1.3. Existing Tensioner Models

Currently, pipelay operations are modeled within the Pipeline Engineering department of Allseas by using simplified descriptions of the tensioner system, which is either:

1. Deadband model, or
2. linear damping with velocity cap model

A deadband model implies that the tensioners start compensating when the tension change reaches the bandwidth and maintain the tension within this limit, irrespective of the rate at which they compensate, which is not a representative of real tensioner behaviour.

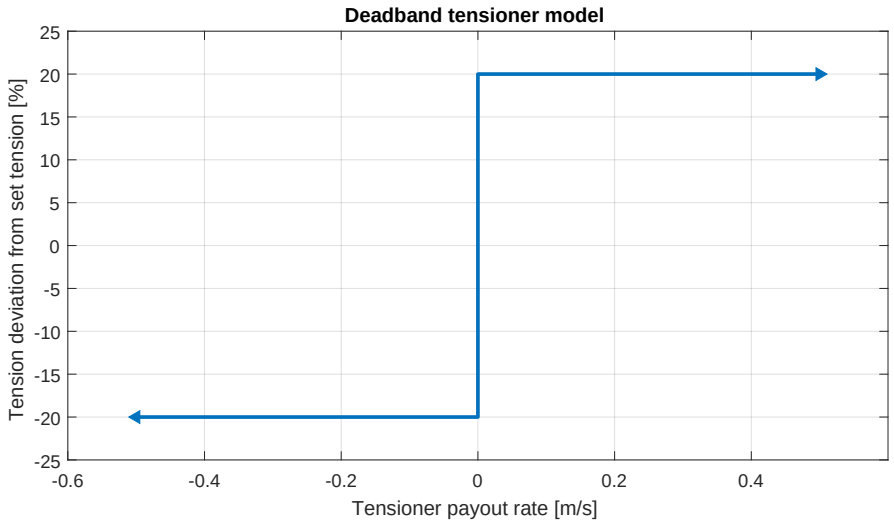

Figure 1.4: Deadband tensioner model

The other model is the linear damping velocity cap. This model implies that the payout rate is linearly proportional to the deviation in pipeline top tension from the set tension, with the maximum payout rate being capped at 0.3 m/s, at which the tensioners speed is maximum.

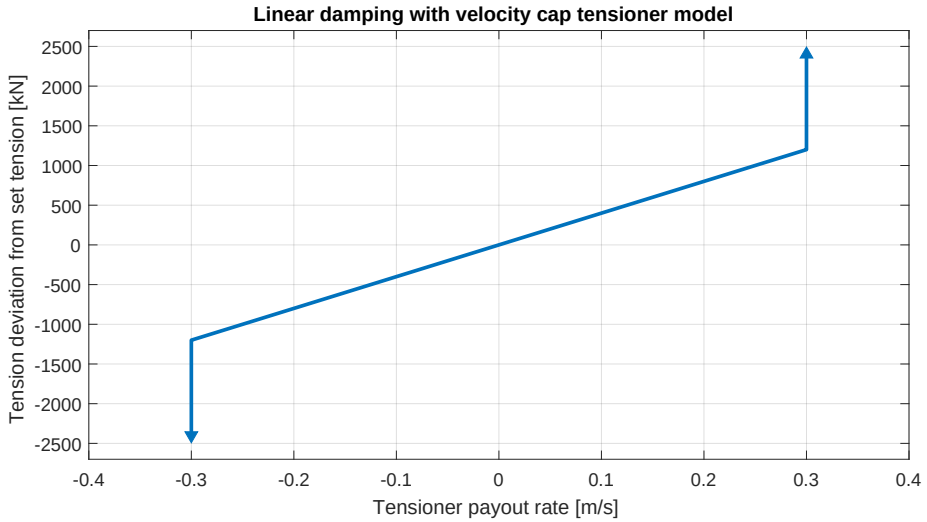

Figure 1.5: Linear damping with velocity cap tensioner model

1.4. Approach

OrcaFlex, which is a finite element package for dynamic analysis of offshore marine systems is used to model the pipelay operations. In total, 7 case studies from shallow to deep water are considered based on full-scale measurement data measured during offshore installation. For each case study, three types of measurement data are available: vessel motions, tensioner pay-out motion and pipeline top tension. Vessel motions and tensioner motion signals are used as inputs to the OrcaFlex model, whereas the measured tension signal is used for comparison with the output pipeline top tension for model validation. The method considered in this thesis is organized into two: 1) model validation and 2) tensioner models comparison.

1.4.1. Model validation

Initially, time history of both the measured vessel motions and tensioner payout motion are used as inputs to OrcaFlex to simulate the real behaviour of the vessel and tensioners during the 3-hour simulation. Subsequently, the model is validated by comparing the output pipeline top tension from simulation with the measured tension.

Before specifying the measurement signals to OrcaFlex, these signals have to be filtered to remove the non-physical components of the signal such as high-frequency components as they are susceptible to measurement noise due to the limited sampling rate of the sensors. Also, to filter components which are not relevant to the study such as low-frequency components of the pay-out signal during pulls. Chapter 2 will discuss in more details about the signal filtering.

Subsequently, the sensitivity study of several parameters which are expected to be influential to tension fluctuation is performed and explained. Based on this, recommendation for future measurement is given. The comparison of the tension signal and sensitivity study will be discussed in Chapter 3.

1.4.2. Tensioner models comparison

After the validation, the specified tensioner motion is removed, and tensioner model is included in the simulation. Now, the tensioner pay-out motion will be computed by the tensioner model based on the pipeline top tension deviation from a set tension at each time step.

In addition to the existing tensioner models described in Section 1.3, a tensioner model with PI controller is introduced. This tensioner model is expected to be the closest representative of the real PI controller of the tensioners system on the vessel. The PI controller model scripted in Python programming language is implemented as an external function of the OrcaFlex model.

Finally, the influence of these tensioner models on pipeline integrity will be given, and conclusion about the tensioner reliability will be drawn.

2

Model Set-up and Methodology

This chapter explains the methodology used in this thesis. First, the theoretical fundamentals used in the thesis are described. Then, an overview of the case studies used for model validation is given. Subsequently, the measurement technique of the data is briefly explained and then explanation about the problem with the measurement signals and digital filter design is given. Then, the process of building the model in OrcaFlex and lastly the signal comparison method is discussed.

2.1. Fundamentals

This section provides the theoretical framework and definitions used in the subsequent chapters. Firstly, the theory of hydrodynamic loads is discussed as it is used when determining the hydrodynamic coefficients, then definition of the maximum von Mises stress and strain will be explained which are used in the pipeline integrity check, subsequently a short introduction to digital signal filtering is given where it is used for signal processing and lastly the theoretical basis of the PID controller and its relevance for the S-lay installation mode is discussed.

2.1.1. Hydrodynamic Forces

The hydrodynamic force F exerted on a pipe segment can be written in terms of the relative acceleration and relative velocity. Morison et al. [2]:

$$F = \rho V \ddot{u} + \rho C_a V (\ddot{u} - \ddot{x}) + \frac{1}{2}\rho C_d A \mid \dot{u} - \dot{x} \mid (\dot{u} - \dot{x}) \tag{2.1}$$

x and u are the pipe displacement and fluid displacement respectively, both in the normal direction of the pipe surface. ρ is density of the surrounding fluid, A is the cross-sectional area of the cylinder perpendicular to the flow direction and V is the volume of the fluid displaced by the pipe segment. For an oscillating cylinder in a still water, the equation can be written as:

$$F = -\rho C_a V \ddot{x} - \frac{1}{2}\rho C_d A \dot{x} \mid \dot{x} \mid \tag{2.2}$$

To obtain an accurate prediction of hydrodynamic forces, the variations of added mass coefficient C_a and drag coefficient C_d should be taken into account as a function of the Reynolds number, the Keulegan-Carpenter number and surface roughness of the pipe.

The parameters are defined as:

$$\begin{aligned} &\text{Reynolds number} : Re = \tfrac{\mathrm{v}D}{\nu} \\ &\text{Keulegan-Carpenter number} : KC = \tfrac{\mathrm{v}_m \cdot T}{D} \\ &\text{Non-dimensional roughness} : \Delta = \tfrac{k}{D} \end{aligned} \tag{2.3}$$

where: D : pipeline outer diameter [m].
T : period of oscillation [s].
k : roughness height [m].
v : relative velocity of fluid particle and pipe[m/s].
υ : fluid kinematic viscosity [m^2/s].
v_m : maximum orbital relative velocity [m/s].

Added mass coefficient

For pipe oscillation in still water, the KC number can be expressed as a function of pipe normal velocity. For a harmonic motion with oscillation frequency ω, $\dot{x}_a = \omega \cdot x_a$, where x_a is the amplitude of the pipe normal displacement and $\dot{x}_a$ is the amplitude of the first derivative of x_a with respect to time, which is the amplitude of the pipe velocity. KC number of pipe oscillation in still water is given by:

$$KC = 2\pi \frac{x_a}{D} \tag{2.4}$$

Hence, the KC number is linearly proportional to the amplitude of lateral pipe motion during half a period. Therefore, this equation also holds for a stochastic pipe motion since it can be expressed as a superposition of an infinite number of harmonic motions. Then, the correlation of KC number and added mass coefficient is shown in Figure 2.1 below from DNV.

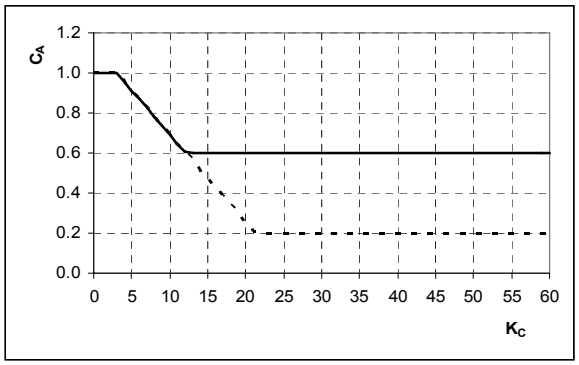

Figure 2.1: Added mass coefficient as function of KC-number for smooth (solid line) and rough (dotted line) cylinder. DNV-RP–C205 [3]

Drag coefficient

Drag coefficients for cylinders depend on the Reynolds number and surface roughness as shown in Figure 2.2.

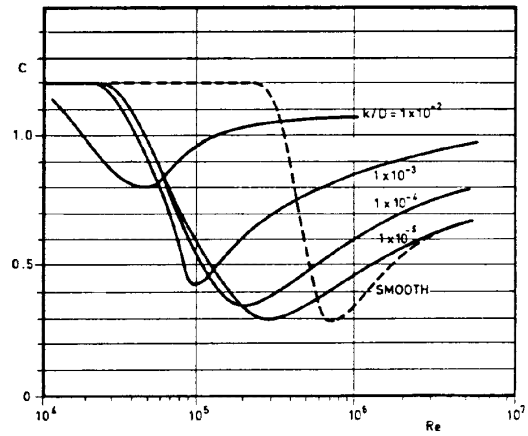

Figure 2.2: Drag coefficient for fixed circular cylinder for steady flow in critical flow regime, for various roughnesses DNV-RP–C205 [3]

Table 2.1: Surface roughness. DNV-RP–C205 [3]

Material	k (meters)
Steel, new uncoated	5×10^{-5}
Steel, painted	5×10^{-6}
Steel, highly corroded	3×10^{-3}
Concrete	3×10^{-3}
Marine growth	$5 \times 10^{-3} - 5 \times 10^{-2}$

While the surface roughness for different coating material is given in Table 2.1

2.1.2. Maximum von Mises Stress

von Mises stress is the equivalent stress due to all types of loading on the pipe section hence it is often used as a yield criterion. In this case, a material is said to start yielding when the von Mises stress reaches the yield strength. von Mises stress is a combination of all the components of the stress matrix and in terms of principal stresses [1], it is given by:

$$\sigma_{vm} = \sqrt{\frac{(\sigma_1 - \sigma_2)^2 + (\sigma_2 - \sigma_3)^2 + (\sigma_3 - \sigma_1)^2}{2}} \tag{2.5}$$

where σ_1 , σ_2 and σ_3 are the principal stresses, i.e. the eigenvalues of the 3 by 3 stress matrix.

$$\begin{bmatrix} \sigma_{RR} & \sigma_{RC} & \sigma_{RZ} \\ \sigma_{RC} & \sigma_{CC} & \sigma_{CZ} \\ \sigma_{RZ} & \sigma_{CZ} & \sigma_{ZZ} \end{bmatrix} \tag{2.6}$$

The three diagonal components of the stress matrix, σ_{RR}, σ_{CC} and σ_{ZZ}, are the radial, circumferential and axial stresses, respectively. While the 6 off-diagonal terms are the shear stresses.

The von Mises Stress varies across the cross section, so its value is reported at a specified position in the pipe section polar coordinates (R,θ) as shown in Figure 2.3.

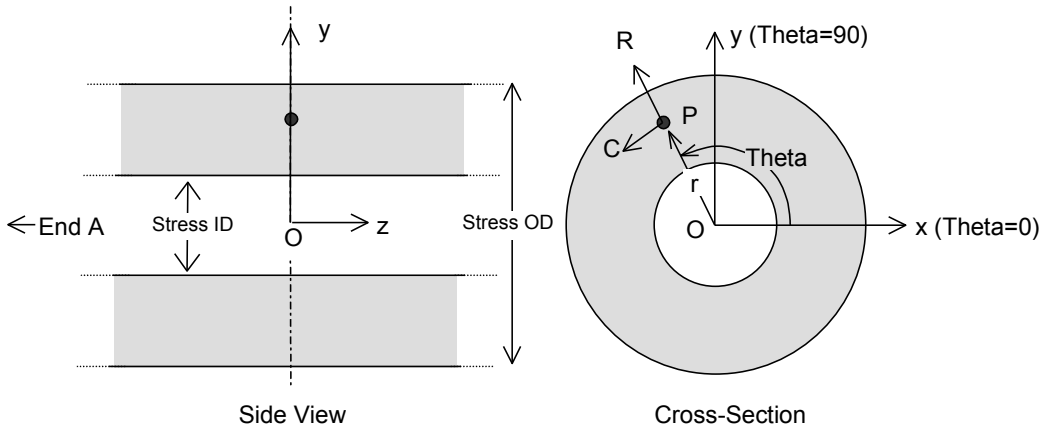

Figure 2.3: Frame of reference for stress calculation [1]

The critical pipeline criteria can be expressed as the maximum von Mises stress, which is an estimate of the maximum value of the von Mises Stress over the cross section. The reported maximum von Mises stress is then taken at coordinate (R,θ) where the value is maximum. For further details about the calculation, the reader is referred to [1]. In the subsequent sections, the maximum von Mises stress will be used as basis for fatigue analysis.

2.1.3. Maximum pipelay von Mises Strain

The pipelay von Mises Strain is a simplified equivalent strain measure commonly used in S-lay analysis. It is given by

$$\epsilon_{vm} = \sqrt{\epsilon_{zz}^2 + \epsilon_{cc}^2 - \epsilon_{zz} \cdot \epsilon_{cc}} \tag{2.7}$$

where ϵ_{zz} is the axial strain, due to direct tensile strain and bending strain, and ϵ_{cc} is the hoop strain, calculated as

$$\epsilon_{cc} = \frac{\sigma_{cc}}{E_{eff}} \tag{2.8}$$

where σ_{cc} is the hoop stress and E_{eff} is an effective Young's modulus, calculated as

$$E_{eff} = \frac{C_2 \cdot EI_{nom}}{I_{xy}} \tag{2.9}$$

where C_2 is the bending stress loading factor and EI_{nom} is the nominal bending stiffness which is defined to be the bending stiffness at zero curvature.

The pipelay von Mises Strain is evaluated at four points in the plane of bending, the inner and outer pipe fibres on each side of the neutral axis of bending, and the maximum of these values is reported.

2.1.4. Fatigue Analysis

The dynamic loading in the pipeline cause the pipeline to accumulate fatigue damage. In order to compute the fatigue damage properly, a realistic tensioner model should be used in the pipelay model. Therefore, the comparison of different tensioner models with respect to fatigue damage will be given.

Fatigue damage of the pipeline is calculated based on the specified S-N curve, which describes the number of cycles to failure $N(S)$, for stress range S. The damage value $D(S)$ is then given by:

$$D(S) = \frac{1}{N(S)} \tag{2.10}$$

This damage value can be thought of as the proportion of the fatigue life that is consumed by 1 cycle of stress range S.

Rainflow-counting algorithm

Firstly, the rainflow-counting algorithm [4] is used to extract the number of cycles and stress ranges from a given stress time history of a pipeline node. The maximum von Mises stress time history is used to calculate the fatigue damage as it is the equivalent stress as explained in Section 2.1.2. The damage from each stress cycle is then summed according to the *Palmgren-Miner rule* to calculate the accumulated fatigue damage experienced by a node $D_{node,3-hour}$ during the 3-hour simulation. Mathematically, this is expressed as:

$$D_{node,3-hour} = \sum_{i=1}^{n} \frac{1}{N(S_i)} \cdot M_i \tag{2.11}$$

Where n is the number of stress ranges and M_i is 0.5 for half-cycles and 1 for full-cycles. For details, the readers is reffered to Maddox S. J. [5] and Rychlik I. [6].

Exposure time

Exposure time is the duration during which a pipeline node is exposed to the load case. During installation, the welding process of a pipe segment to the suspended pipeline takes around 10 minutes duration. During this period, the pipeline stays in position and is subjected to cyclic loading leading to fatigue damage. After the welding process is finished, the pipeline is paid out therefore a new welding process can be started. This paying out is referred as *pulls* in pipelay industry.

Due to these pulls, each node of the pipeline is actually subjected to the load case only for 10 minute duration. Therefore, the accumulated fatigue damage from the 3-hour simulation, $D_{node,3-hour}$ is scaled linearly to 10 minute duration as expressed equation 2.12.

$$D_{node,exposure} = D_{node,3-hour} \cdot \frac{\text{exposure time}}{3} \tag{2.12}$$

Where the unit of the exposure time is in hour.

Accumulated fatigue damage of pipe joints

Since the pipeline node spacing in the OrcaFlex model is not the same as the pipeline joint spacing in reality, the fatigue damage at each pipe joint is obtained by linear interpolation. In this project, the length of a pipe segment is 12.2 meters. Therefore, the accumulated fatigue damage at each pipe joint during the exposure time $D_{joint,exposure}$ is obtained by interpolation of fatigue damage at pipeline node at every 12.2 meters.

Total accumulated fatigue damage of a pipe joint

As the pipeline is paid out during each pull, a pipe joint is subjected to a different load case every 10 minutes, depend on the position along the catenary. At the end of the installation when the pipe joint completely rests on the seabed, this pipe joint has been accumulating fatigue damage starting when it left the tensioners on the vessel until it reached the seabed.

The total accumulated fatigue damage experienced by a pipe joint $D_{joint,total}$ in the installation phase is calculated as the sum of the accumulated fatigue damage at each position step starting from the tensioners to the seabed. In the model, this is basically the summation of all the accumulated fatigue damage during the exposure time $D_{joint,exposure}$.

Allowable standby time

In addition, more fatigue damage may be consumed by the pipeline when the installation process is temporarily stopped due to unexpected accidents, welding repair, and in-line structure welding, etc. During these events, the pipeline will be held in position and exposed to more dynamic loading cycles. During this stationary period, the node with the largest accumulated fatigue damage determines how long the pipe can be held in a stationary position at the worst node; this is referred to as the allowable standby time.

$$\text{Allowable standby time} = \frac{\text{Allowable fatigue damage} - D_{joint,total}}{Drate_{worst\ node}} \tag{2.13}$$

Where $Drate_{worst\ node}$ is the accumulated damage rate per hour at the worst node. The worst node is the node where $D_{node,3-hour}$ is at the maximum. The $Drate_{worst\ node}$ is expressed in equation 2.14 below.

$$Drate_{worst\ node} = \frac{max(D_{node,3-hour})}{3} \tag{2.14}$$

2.1.5. Digital Signal Filtering

A digital filter is a system that performs mathematical operations on a discrete-time signal to reduce or enhance certain aspects of that signal. It is often described by its frequency response. The three most common types of filters (ideal filters) are the *lowpass*, *highpass* and *bandpass* as illustrated in Figure 2.4

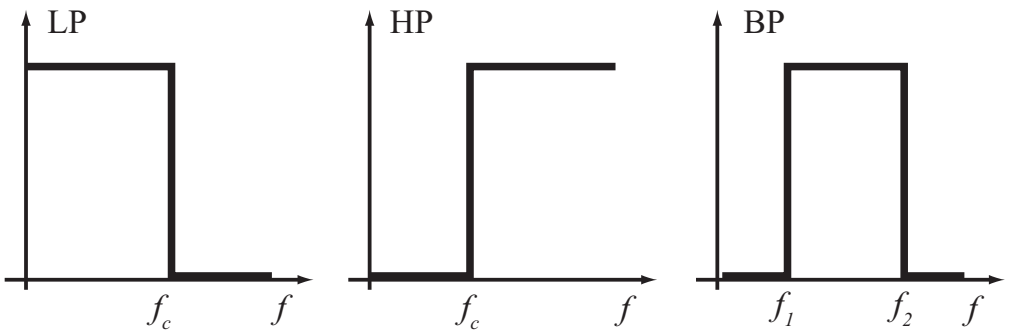

Figure 2.4: Ideal filter characteristics. 'LP' indicates the characteristic of an ideal lowpass filter, 'HP' the ideal highpass filter characteristic, and 'BP' the ideal bandpass characteristic. [7]

As the names imply, the lowpass filters let low frequencies pass, and consequently high frequencies are filtered out. Similarly, the highpass filter is used to filter out low frequency components, whereas for the bandpass filter all frequencies, except those in the passband region, are filtered out.

However, the ideal filters cannot be physically realized. With digital filter designs, however, it is possible to get close to ideal characteristics, at the expense of two sorts, namely computational cost, and time delay. For further details about filter design, the reader is referred to Anders Brandt [7].

In frequency domain, the frequency response can be seen as a transfer function characterized as linear, time-invariant (LTI) systems. The output spectrum is the multiplication of the frequency response with the input signal amplitude spectrum. Subsequently, inverse Fourier transform can be used to obtain back the output signal. In time domain, it can be seen as the linear convolution of the input signal with the filter impulse response, where the impulse response is the filter output for a unit impulse input. This impulse response is well-known as filter coefficients.

In this thesis, two types of digital filter are used, which are the low-pass filter and band-pass filter. Both filters are designed by using the built-in function *designfilt* in Matlab. For more details the reader is referred to MathWorks [13].

As an example, the band-pass filter design will be discussed. Firstly, the filter properties such as type of filter, filter order, cut-off frequencies, design method and sampling rate of the input signal are specified as shown below.

```
bpFilt = designfilt('bandpassfir', ...          % Response type
       'FilterOrder',2000, ...                  % Filter order
       'StopbandFrequency1',1/low_fc-0.005, ... % Frequency constraints
       'PassbandFrequency1',1/low_fc+0.005, ...
       'PassbandFrequency2',1/high_fc-0.005, ...
       'StopbandFrequency2',1/high_fc+0.005, ...
       'DesignMethod','ls', ...                 % Design method
       'StopbandWeight1',1, ...                 % Design method options
       'PassbandWeight', 4, ...
       'StopbandWeight2',1, ...
       'SampleRate',1/tstep) ;                  % Sample rate
```

The values specified in the frequency constrains depend on the cut-off frequency. These constrains are chosen to be in the neighbouring of the cut-off frequency. These are required in order to have a smooth transition from the pass band frequency to the stop band frequency of the filter. To have a narrower frequency constraints, a higher filter order is required, thus results in more computational time. On the other hand, the frequency constraints should be chosen narrow enough so that the pass-band and stop-band frequency do not deviate from the desired bands.

Subsequently, the frequency response of the designed filter is multiplied with the amplitude spectrum of the input signal. Alternatively, in time domain, linear convolution of the filter coefficients and the time history of the input signal is performed. This is done by the *filtfilt* function which is intended for zero-phase digital filtering as shown below.

```
output = filtfilt(bpFilt,input);
```

2.1.6. PID Control Theory

The name of PID control implies its three correcting terms: proportional, integral and derivative. The summation of these terms is defined as the controller output. Mathematically, the input-output relation for an ideal PID controller with error feedback is:

$$u(t) = k_p \cdot e(t) + k_i \cdot \int_0^t e(\tau)d\tau + k_d \cdot \frac{de}{dt} = k_p\left(e(t) + \frac{1}{T_i}\int_0^t e(\tau)d\tau + T_d\frac{de}{dt}\right) \tag{2.15}$$

The controller parameters denoted by the proportional gain k_p, the integral gain k_i and the derivative gain k_d. PID Controller continuously calculates an error value $e(t)$ as the difference between a desired set point r and a measured value as the output of the system $y(t)$. Based on the controller gains, PID controller applies a corrective action to reduce the error value to the system $P(s)$. Schematically the closed-loop system is illustrated in Figure 2.5 below,

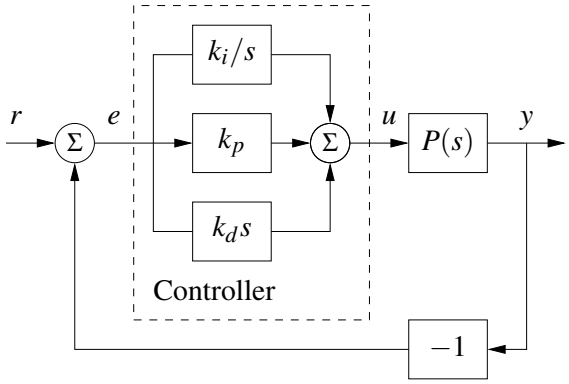

Figure 2.5: PID using error feedback. [8]

In practice, not all of these three terms in equation 2.15 should be present. For instance, the control system which is used for the tensioners on *Solitaire* is a PI controller.

For the S-lay installation mode, the system $P(s)$ can be seen as the mechanical system of the offshore pipelaying comprises the suspended pipeline with 2 boundary conditions at both ends, interaction along the interface with the seabed, fluid, and stinger. The controller setpoint r is the desired pipeline top tension that is intended to be maintained. The system output $y(t)$ is the observed pipeline top tension as the result of disturbance by the vessel motions. Lastly, the control output $u(t)$ is the payout rate produced by the tensioners. As a comparison, the process is illustrated in Figure 2.6 below.

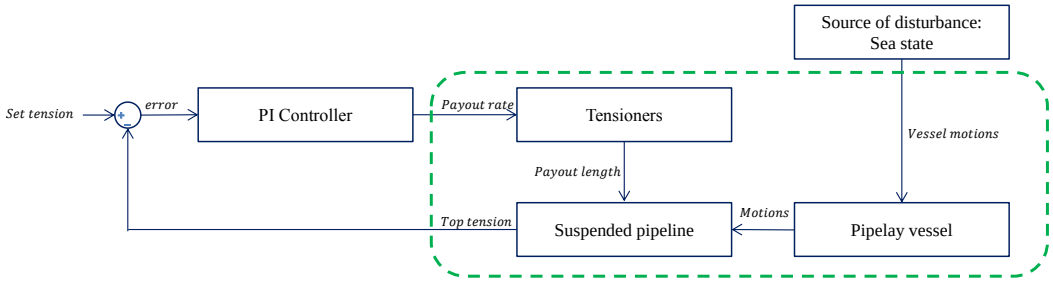

Figure 2.6: Mechanics of an active S-lay pipeline installation.

2.2. Overview of the Case Studies

Polarled project which is installed by Allseas' pipelay vessel *Solitaire* is considered in this thesis. The pipeline consists of a 36" pipeline section which transports a dry, rich gas operating in the dense phase, i.e. as single phase gas with a total pipeline length of 482 km, starting from Aasta Hansteen towards the landfall at Nyhamna.

During installation, the vessel position along the installation route is recorded daily in the Daily Progress Report (DPR) document. Considering this information and the payout measurement, the vessel position at a specific time can be obtained. Once the vessel position is known, case specification such as water depth, pipe properties, and soil properties are known.

Case studies considered in this thesis ranges from shallow water at 112 meters to deep water at 774 meters with various sea states and pipe properties as illustrated in Figure 2.7.

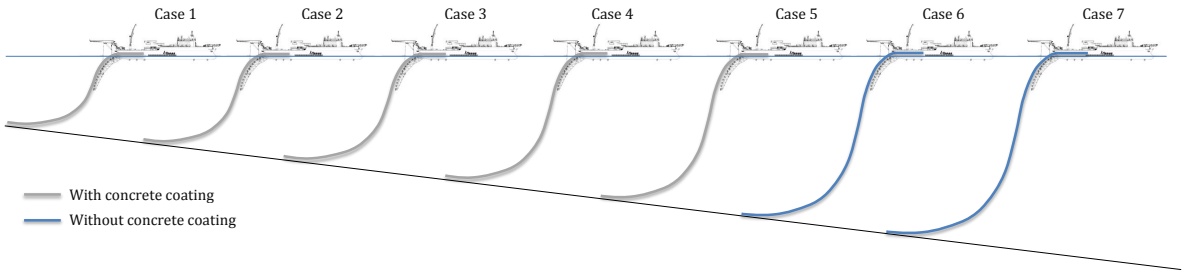

Figure 2.7: Overview of the case studies

The characteristic for every case can be seen in Table 2.2 below,

Table 2.2: Overview of the case study characteristics

Parameters	Case 1	Case 2	Case 3	Case 4	Case 5	Case 6	Case 7
Significant wave height [m]	3.9	2.1	1.6	1.2	1.4	1.4	1.3
Water depth [m]	112	238	354	554	694	704	774
Max. heave [m]	1.7	1.5	0.8	0.7	0.8	0.8	0.7
Max. pitch [m]	0.8	0.7	0.7	0.4	0.4	0.4	0.4
Max. surge [m]	0.4	0.6	0.4	0.4	0.3	0.3	0.3
Pipe inner diameter [mm]	854	854	854	854	854	854	854.0
Pipe wall thickness [mm]	30.5	30.5	28.9	28.9	28.9	34.6	34.6
Concrete coating density [kg/m3]	3050	2250	2250	2250	2250	-	-
Concrete coating thickness [mm]	70	50	50	50	50	-	-
Set tension [kN]	2219	1383	1615	2746	3269	1523	1653.0

From case 1 to case 5 the pipe is coated with concrete coating to provide weight during installation and protection during operation. Case 6, which is in the deepest water is not coated with concrete,instead it has a thicker pipe wall thickness.

2.3. Measurement Data and Filter Design

Measurement data are recorded in real time on the vessel by a number of sensors and then stored in the Datalogger. Prior to setting up the model for a case study in OrcaFlex, the measurement data have to be preprocessed to remove components of the signals which are not physical or not relevant to the study. In this chapter, the measurement data from case 4 are used to describe the data processing while the data for the other cases can be seen in Appendix A.

2.3.1. Vessel Motions

Solitaire's vessel motions in 6 degrees of freedom are measured over time by the Motion Reference Units (MRU), which comprises of multiple gyroscopes and accelerometers. The MRUs are placed at a distance from the vessel's center of motions, hence the vessel motions data have to be corrected by the lever arms before used as input to OrcaFlex. The vessel motions data for *Solitaire* in the Datalogger are available in two types: original data at the MRUs location and data with lever arms applied, which is used in this thesis.

The amplitude spectrum is shown in Figure 2.8 below. The measured vessel motions comprise of all kinds of loads experienced by the vessel during operation such as wave loads, current loads and weight due to pipe loading and storage at one side of the vessel.

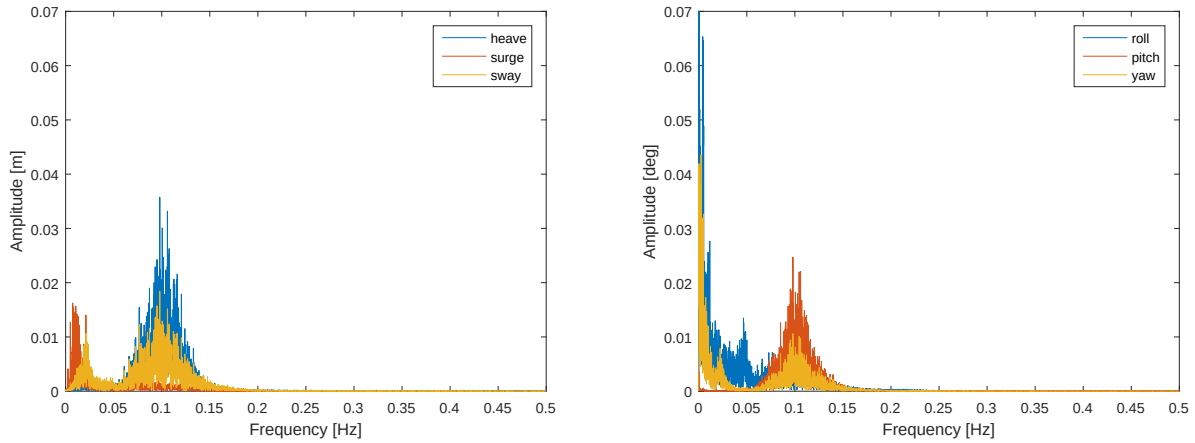

(a) Translational motions

(b) Rotational motions

Figure 2.8: Amplitude spectrum of vessel motions

The wave-induced vessel motions can be split into the first and second order vessel motions. The first order vessel motions can be seen at the wave frequency, in the amplitude spectrum they are located at around 0.1 Hz. Subsequently, the second order vessel motions are located at a lower frequency. This can be seen in the roll motions at 0.05 Hz and both surge and sway motion at around 0.025 Hz.

Besides motions generated by waves, the vessel also experienced specific loads for a pipelay vessel such as pipe loading and storage on one side of the vessel which leads to drift in the roll motions.

In the high-frequency range (larger than 0.2 Hz) the amplitudes are relatively small. This is due to the fact that vessel motions can be seen as rigid body motion with a large inertia thus it is unlikely to have high-frequency components. Therefore, to remove the non-physical components in the high-frequency, a low-pass filter with cut-off frequency of 0.2 Hz is used before specifying the vessel motions to OrcaFlex.

2.3.2. Tensioner Payout

Tensioner motion is described by the payout motion it produced to displace pipeline. This payout motion is measured during offshore installation. OrcaFlex, however, requires payout rate as the input state for the tensioner motions. Payout rate can be obtained by taking the first derivative of the payout with respect to time.

The measured payout rate signal is shown in Figure 2.9. During the first 6800 seconds, the tensioner is compensating the tension by paying out and hauling in the pipeline with a relatively low amplitude. Afterwards, besides compensating, the tensioners are also paying out pipeline with a relatively large rate compared to the compensating payout rate. This phenomenon is known as *pulls*, during which the tensioners

are paying out pipeline towards the seabed after the welding process of a new pipe section to the suspended pipeline.

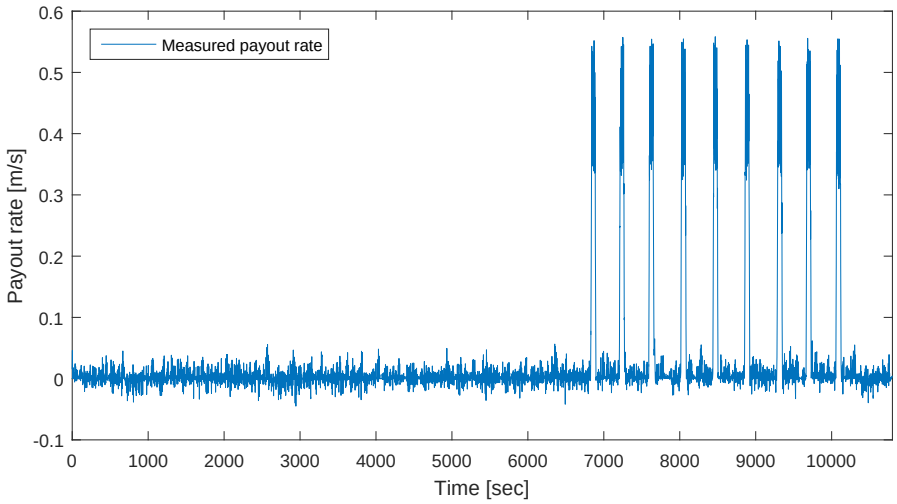

Figure 2.9: Tensioner payout rate

A part of the payout rate signal during a pull is shown in Figure 2.10. While paying out pipeline the vessel is also moving forward. The process continues until the end of the installation route.

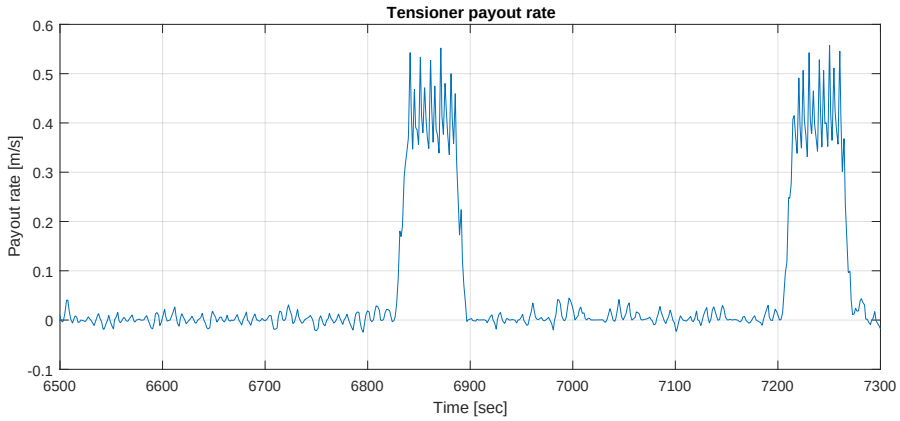

Figure 2.10: Tensioner payout rate during a pull

The amplitude spectrum of the payout rate signal is shown in the figure below. Figure 2.11a shows the amplitude spectrum of the last 4000 seconds of the time history and Figure 2.11b shows the amplitude spectrum for the first 6800 seconds, during which there was no pulls is observed.

As expected, the payout rate also contains low-frequency components induced by the low-frequency vessel motions. However, in contrast with vessel motions, the payout rate during pulls also contain peaks in the high frequencies as shown in Figure 2.11a.

As a comparison, the amplitude spectrum of the first 6800 seconds where the vessel is in the steady state condition, does not contain any peaks with significant magnitude after the first peak at 0.1 Hz.

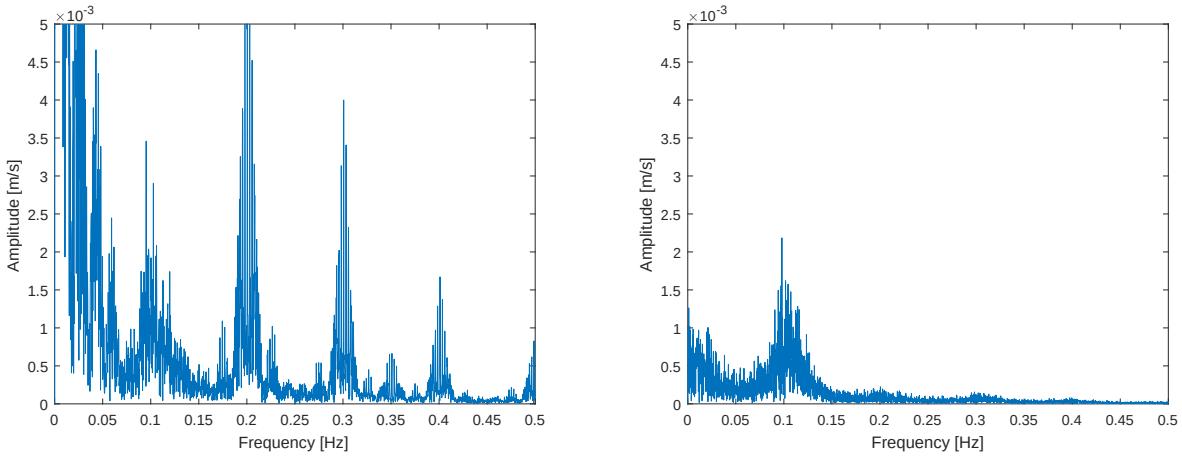

(a) With pulls

(b) Without pulls

Figure 2.11: Payout rate amplitude spectrum

A digital band-pass filter is required to remove the low-frequency and high-frequency components of the payout rate signal, which happened during pulls. Pulls are not relevant for the study and it should be removed from the signals. Considering the amplitude spectrum, the band-pass filter is designed with low-frequency cut-off at 0.05 Hz and a high-frequency cut-off at 0.14 Hz. Result of the signal filtering can be seen in Figure 2.12 below.

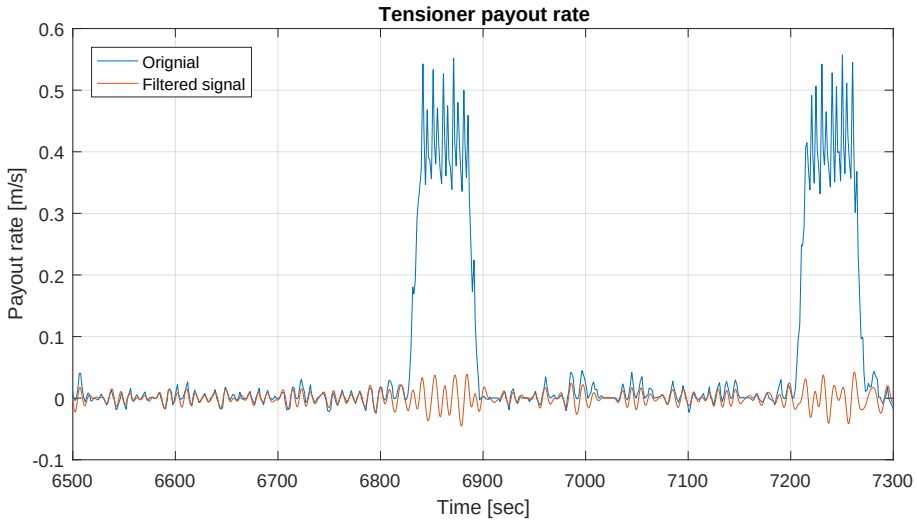

Figure 2.12: Time domain comparison of filtered and unfiltered signal

2.3.3. Pipeline Top Tension

Pipeline top tension is measured by load cells which are mounted at each tensioner track. In Solitaire, there are 3 tensioners hence assuming the tensioners are aligned and the load cells are calibrated properly, the total pipeline top tension is the summation of the time trace from 12 load cells measurement. The amplitude spectrum of the total pipeline top tension is shown in Figure 2.13 below.

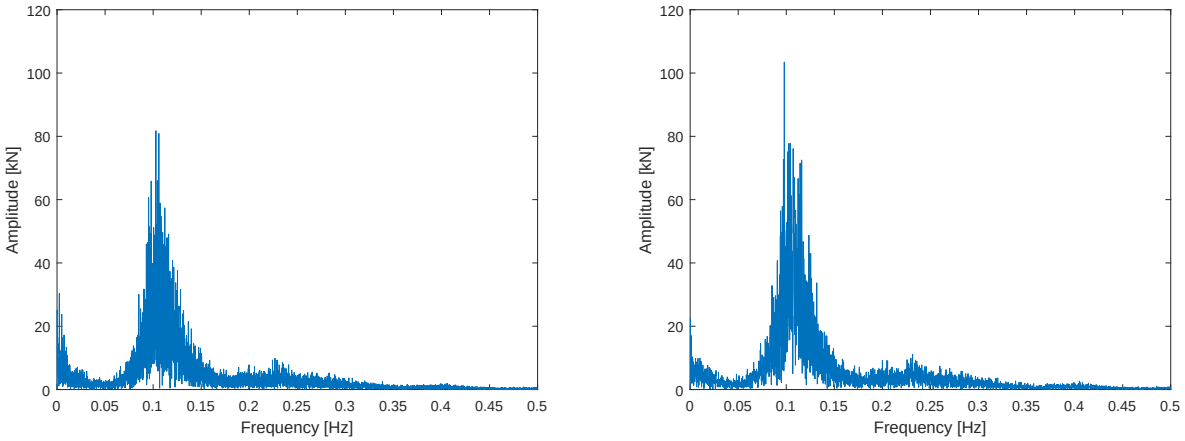

(a) With pulls

(b) Without pulls

Figure 2.13: Measured tension amplitude spectrum

As can be seen in Figure 2.13, the tension signal also contains low-frequency components which correspond to pulls, hence a low-frequency cut-off used for the band-pass filter is also at 0.04 Hz. In the high frequencies, the two amplitude spectra are almost identical, where the signal with pulls does not contain high-frequency peaks. Therefore a band-pass filter with a high-frequency cut-off of 0.20 Hz can be used as also used for the vessel motions.

2.4. Model Setup in OrcaFlex

S-lay installation technique can be modelled by considering the suspended pipeline as an axially tensioned geometrically non-linear beam subject to axial loads, lateral loads and motions at the upper end induced by the pipelay vessel. Mathematically, this is a non-linear partial differential equation that cannot be solved analytically. Also, frequency domain analysis would not adequately predict the pipeline behaviour due to the nonlinear dynamic response of the pipeline. Despite the fact that many of the concepts for state space modelling and analysis can be used for non-linear systems, frequency domain analysis applies primarily to linear systems. For that reason, time domain analysis is chosen to be performed in this thesis.

A model for S-lay pipeline installation consists of a pipelay vessel, stinger, tensioners, suspended pipeline and seabed model. In the following section, the model set-up in OrcaFlex is explained.

2.4.1. Pipeline model

During S-lay installation, the suspended pipeline is subjected to various loads such as hydrodynamic loads, internal and external pressure, vessel motion-induced loads, pipeline weight, buoyancy and resistance force due to contact with the seabed. An overview of the various type of internal forces and moments due to these loadings is given in Figure 2.14 below,

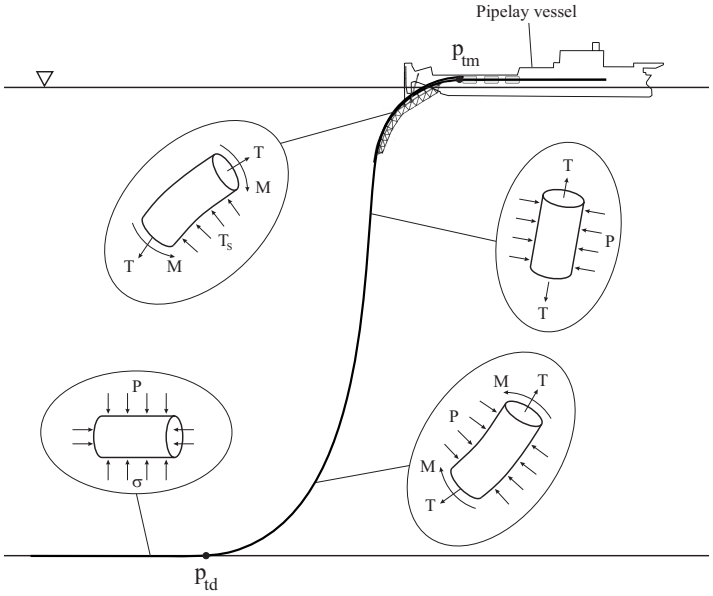

Figure 2.14: Loadings during S-lay Installation. T indicates the axial tension in the pipeline, M is the bending moment, P represents the external pressure, T_s is the contact force with the stinger and σ represents the contact stress with the seabed.

Pipeline is modeled in OrcaFlex as a beam element discretized by using the finite element method. Specifically, it is modeled as a first order beam element, which is also known as a "lumped mass" model as shown in figure 2.15a. Each element is modelled as a massless segment with one node at each end. Properties that are related to the inertia such as mass, buoyancy and additional weight of the element are lumped into the node. OrcaFlex works in 6 degrees of freedom of the element as illustrated in the detailed structural model below,

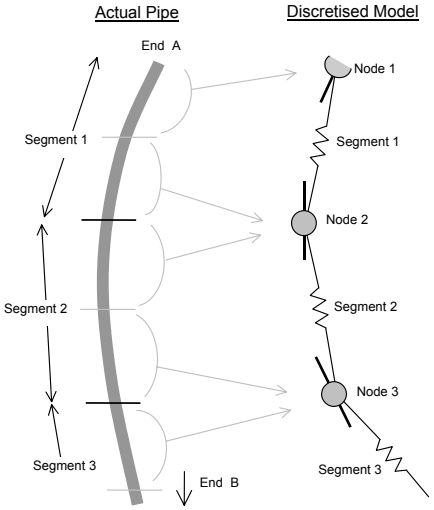

(a) Simplified structural line model in OrcaFlex

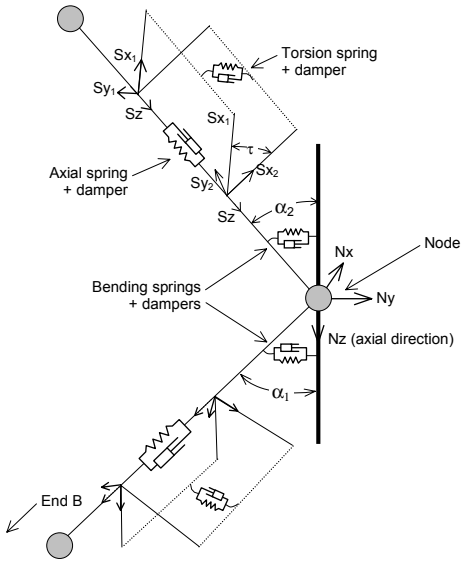

(b) Detailed structural line model in OrcaFlex

Figure 2.15: Pipeline discretization in OrcaFlex

1. In the axial direction, stiffness, and damping of the pipeline are modelled by the axial spring and damper at the center of each segment, which applies an equal and opposite axial force to the end nodes.

2. Bending properties of the pipeline are modelled by rotational spring and dampers either side of the node, spanning between the node's axial direction N_z and the segment's axial direction S_z.

3. Torsional stiffness and damping are modelled by the torsional spring and damper at the center of each segment, which applies equal and opposite torque moments to the nodes at each end of the segment.

2.4.2. Vessel Model

Pipeline-vessel interaction is the most complex among the other pipeline interactions. This is due to the pipelay vessel comprised of several types of equipment such as stinger, roller boxes, tensioners which are influential to the suspended pipeline dynamics. A proper vessel model requires the vessel dimension data, draft during operation, the configuration of the stinger, position of the roller boxes and the vessel motions reference point locations.

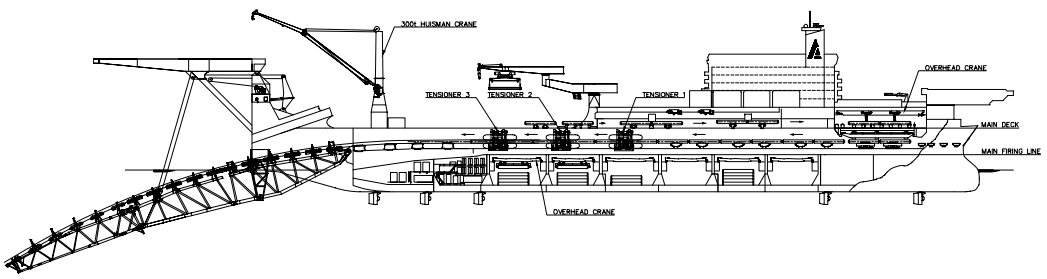

Figure 2.16: Solitaire pipelay vessel

In this thesis, the pipelay vessel is based on *Solitaire*, which is one of the largest pipelay vessels in the world owned by Allseas. The dynamically-positioned pipelay vessel measures 397 m in length and 41 m in breadth.

In general, a pipelay vessel has 6 degrees of freedom at the center of motions: 3 translations (surge, sway, heave) and 3 rotations (roll, pitch, yaw). The measured vessel motions is used as inputs to simulate the real behaviour of the vessel during offshore installation.

Careful attention should be given to the vessel's convention such that the conventions used by the measurement match the convention used in the model. The conventions shown in Figure 2.17 illustrate the synchronized convention.

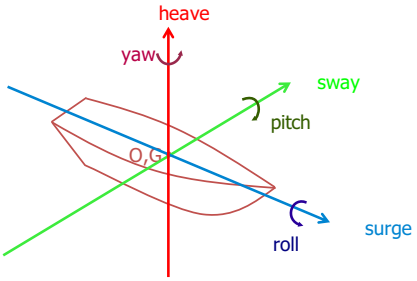

Figure 2.17: Vessel motions convention

In addition, careful attention should also be given to the location at which the vessel motions are superimposed. As discussed in the previous chapter, the vessel motions have been corrected with the lever arm applied, which means that the vessel motions are the motions at the vessel's center of motions. For *Solitaire*, the center of motions coincides with the vessel reference point at which vessel RAOs are defined, which also coincides with the vessel's Centre of Gravity (CoG).

2.4.3. Stinger

Stinger is made up of truss structures hinged off the back of the pipelay vessel. This stinger provides supports to the suspended pipeline during the transition from the vessel into the water.

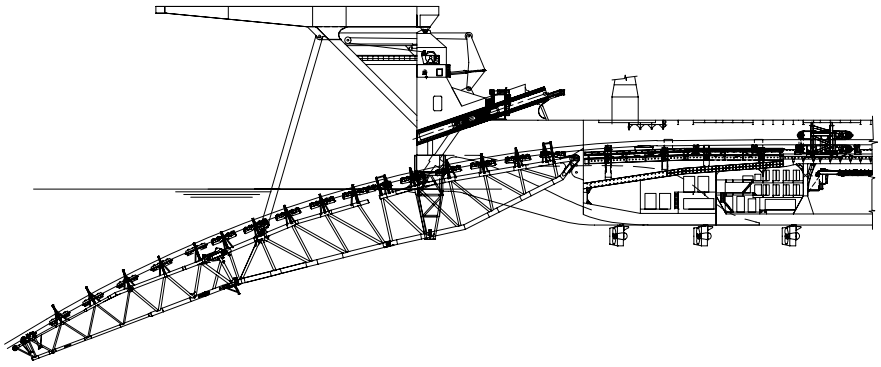

Figure 2.18: Stinger

Along the stinger and firing line, pipeline is supported by roller boxes. The configuration of these roller boxes is explicitly specified in OrcaFlex based on the stinger configuration for a specific case. In all cases considered in this thesis, the stinger configuration is the same, therefore the vessel model is identical for all cases.

2.4.4. Tensioners

To simulate the tensioner behaviour, pipeline's end on the vessel is connected to a winch element. Winches provide a way of modelling the tension compensating mechanism by hauling in or paying out motion. Basically, a winch element is a wire element with a certain stiffness and damping value. As can be seen in figure 2.19, winch connects two (or more) nodes of objects in the model by a winch wire which is then driven by a winch drive.

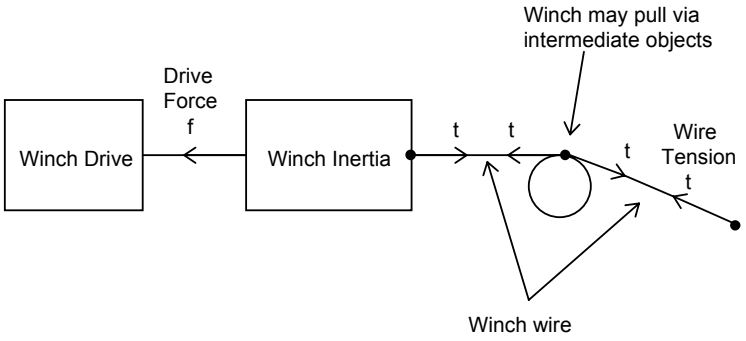

Figure 2.19: Winch Model

There are two modes of operation of a winch in OrcaFlex:

1. Specified payout rate: the payout motions of the winch wire is specified. The value can be fixed, vary with simulation time or be given by an external function. While the winch tension is the output of the simulation.

2. Specified tension: the tension of the winch wire is specified. This value can be fixed, vary with simulation time or be given by an external function. The payout is then adjusted to obtain the target tension.

Prior to modelling the controller, the measured payout rate is specified to simulate the tensioner behaviour and the output tension is compared to the measured tension. This mode is chosen because in reality the output of the PI controller on the vessel is also the payout rate, while tension is the result of the pipelaying dynamics. In addition, payout motion is parameter that can be controlled and solely generated by the controller. While pipeline top tension is more complex as it is combination of various components such as hydrodynamic loads, rollers friction, soil friction, tensioner behaviour and vessel motions.

2.4.5. Seabed Model

The non-linear hysteretic seabed model proposed by Randolph M. and Quiggin P. [9] is adopted by OrcaFlex to model the dynamic pipeline-seabed interaction. This non-linear seabed model captures the essence of varying soil stiffness with the magnitude of pipeline penetration and cyclic motions. As penetration increases or decreases, then the resistance asymptotically approaches the ultimate penetration resistance $P_u(z)$ or the ultimate suction resistance $P_{u\text{-}suc}(z)$ respectively. Both asymptotic limits are defined as

$$\begin{aligned} P_u(z) &= N_c(z/D)s_u(z)D \\ P_{u-suc}(z) &= -f_{suc}P_u(z) \end{aligned} \tag{2.16}$$

where $s_u(z)$ is the undrained shear strength at penetration z, $N_c(z/D)$ is the bearing factor, f_{suc} is the non-dimensional suction resistance ratio parameter, coefficients a=6 and b=0.25 were suggested by Randolph M. and White [10].

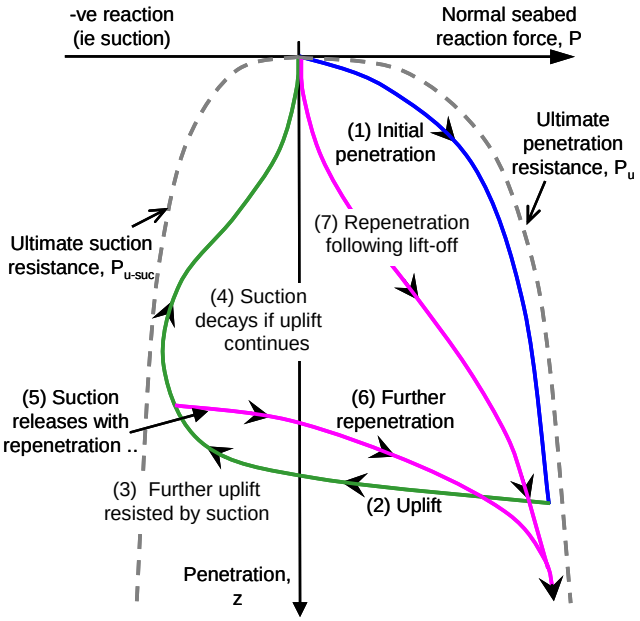

Figure 2.20: Soil model characteristic for different modes. [9]

The undrained shear strength profile of the soil is determined based on project geotechnical investigation report [11]. The values for each case study is taken from the closest location where geotechnical data are available. They are given in Table 2.3 below.

Table 2.3: Parameters for calculation of undrained bearing capacity with linearly increasing shear strength

Parameters	Case 1	Case 2	Case 3	Case 4	Case 5	Case 6	Case 7
KP at touchdown point	439.10	353.36	75.82	45.42	38.52	37.15	36.01
Undrained shear strength at base level, [kPa]	1.504	1.41	1.692	1.692	1.692	1.692	1.692
Increase in undrained shear strength, [kPa/m]	0.8	0.8	0.8	0.8	0.8	0.8	0.8

In addition, a moderate value of soil friction coefficient for pipeline on soft clay of 0.55 is implemented. The other parameters related to suction resistance, soil buoyancy, cyclic uplift and repenetration are assumed to be the default values used by Randolph M. and Quiggin P. [9].

2.4.6. Hydrodynamic Coefficients

As explained in Section 2.1.1, the added mass coefficients can be approximated by the Keulegan-Carpenter number. However, it requires an iterative procedure to determine an appropriate added mass coefficient. The iterative procedure to calculate the Keulegan-Carpenter number is as follows:

1. Initially the theoretical value for added mass coefficient of 1.0 for zero $Kc = 0$, is assumed.
2. From the initial simulation, pipe motions in the normal direction at each node are extracted from the model. The 2 local axes x and y at which pipe motion in OrcaFlex are defined. This is shown in Figure 2.21.
3. Then, the resultant of these two motions $u(t)$ is calculated simply by using the Pythagorean theorem.
4. Variations of KC number are then computed based on the pipe outer diameter and variations of the normal pipe motions $u(t)$ as expressed in equation 2.4.
5. Subsequently a range graph of the KC number is obtained.

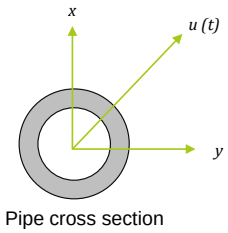

Figure 2.21: Pipeline local axes orientation

As an example, KC number from Case 4 is shown in Figure 2.22. The minimum value correspond to the small amplitudes in the pipeline motions. These small amplitudes do not create significant disturbance to the surrounding fluid and therefore it can be neglected when calculating KC number. The significant dynamic amplitude is taken within the range between the mean and the maximum value. Based on this, the design value for the KC number is taken as the average between the mean and maximum value of the KC number.

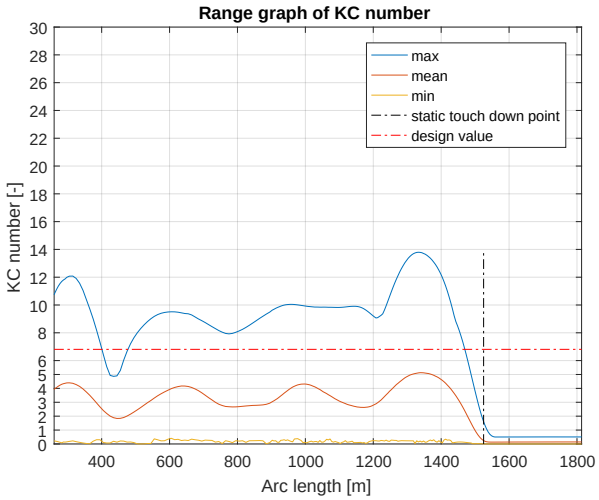

Figure 2.22: Range graph of KC number

Based on the design value, pipeline added mass coefficient is then determined referring to Figure 2.1. Subsequently, added mass coefficient in the model is updated with the calculated coefficient. Results from the other cases can be seen in Appendix ch:Appendix.

Drag coefficient of the pipeline depends on the Reynolds number as shown in Section 2.1.1. Therefore, the drag coefficient is changing over time. However, simplification can be made by using a constant drag coefficient which is explained in Section 3.2.4

2.4.7. Static Configuration

Prior to conducting a dynamic analysis, the static configuration of the OrcaFlex model has to be set properly. As can be seen in Figure 2.23, the OrcaFlex model consists of a pipeline that is fixed to the vessel at the upper end and pinned to the seabed at the lower end. The pinned point location is chosen far enough from the touchdown point such that the dynamic motions of the pipeline at this point is relatively low thus can be neglected. This requires an iterative procedure, but in most cases, 1 kilometre from the touch down point should be sufficient.

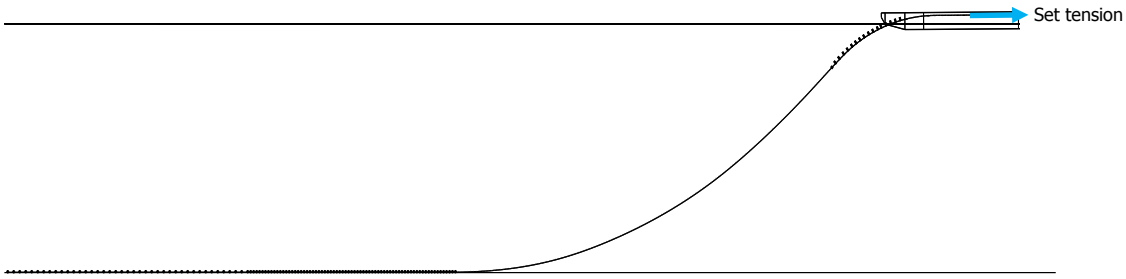

Figure 2.23: Static configuration set-up

For a specific installation case, water depth and coordinates of the pipeline ends are known. Therefore, the only unknown is the pipeline length between these two boundaries. Mechanically, this pipeline length governs the static tension (set tension) in the pipeline. Therefore, these two parameters shows input-output relation for a pipelay model. For a chosen pipeline length, set tension will be the output of the static calculation and vice versa, OrcaFlex iterates the suspended length to obtain a desired set tension.

During offshore operation, it is more practical to measure the pipeline top tension rather than the suspended length, which is the distance from the upper end to the touch down point. In fact, pipeline top tension is measured during installation. For this reason, the static configuration is determined based on the measured pipeline top tension. The static part of the measured tension signal, which is the mean value is used to determine the static configuration.

This approach is indeed only valid if ocean current force is negligible as current force affects the mean value of the tension signal. Due to the unavailability of current measurement or stinger tip clearance measurement, this approach is used to determine the static configuration. In the next chapter, the implication of this decision is explained and the effect of current on tension is discussed.

2.4.8. Integration Method for Dynamic Analysis

In the time domain dynamic simulation, OrcaFlex implements two integration methods, Explicit and Implicit, as described below. Both methods recompute the system geometry at every time step and so the simulation takes full account of all geometric non-linearities and load variations.

Equation of motion

The equation of motion of the system modelled in OrcaFlex is shown below.

$$M(x,\ddot{x}) + C(x,\dot{x}) + K(x) = F(x,\dot{x},t) \tag{2.17}$$

where:
- $M(x,\ddot{x})$: system inertia load.
- $C(x,\dot{x})$: system damping load.
- $K(x)$: system stiffness load
- $F(x,\dot{x},t)$: external load.
- x, $\dot{x}$ and $\ddot{x}$: position, velocity and acceleration vectors respectively.
- t : simulation time.

Explicit Integration Scheme

At beginning of the simulation, the initial state (positions and orientations) of all objects in the model, including all pipeline nodes, are known from the static analysis. The forces and moments acting on each free body and pipeline node are then calculated. Forces and moments considered include:

1. weight
2. buoyancy
3. hydrodynamic and aerodynamic drag
4. hydrodynamic added mass effects, calculated using the usual extended form of Morison's Equation with user-defined coefficients
5. tension and shear
6. bending and torque
7. seabed reaction and friction
8. contact forces with other objects
9. forces applied by links and winches

The equation of motion (Newton's law) is then formed for each free body and each pipeline node in the local axes.

$$M(x) \cdot \ddot{x} = F(x, \dot{x}, t) - C(x, \dot{x}) - K(x) \tag{2.18}$$

This equation is solved to obtain the acceleration vector $\ddot{x}$, and then the semi-implicit Euler integration is used to obtain the system state at the new time step.

To express this mathematically, the position, velocity and acceleration at time t are denoted by $x(t)$, $\dot{x}(t)$ and $\ddot{x}(t)$ respectively. Then, the state at the next time step $(t + dt)$ are given by:

$$\begin{aligned} \dot{x}(t + dt) &= \dot{x}(t) + dt \cdot \ddot{x}(t) \\ x(t + dt) &= x(t) + dt \cdot \dot{x}(t + dt) \end{aligned} \tag{2.19}$$

At the end of each time step, the state of all nodes and free bodies are again known and then these new state is used as initial condition for the next time step. The process is repeated until the end of simulation time.

Implicit Integration Scheme

In the implicit integration scheme, OrcaFlex uses the Generalised-α integration scheme as described by Chung J. and Hulbert G. M. [12]. The forces, moments, damping, mass etc. are calculated similarly as for the explicit scheme.

The implicit scheme solves the equation of motion involving both the current state of the system and the later one at the next time step. Because x, $\dot{x}$ and $\ddot{x}$ at the next time step are unknown, an iterative solution method is required. Consequently each implicit time step consumes significantly more computation time than an explicit time step. Implicit scheme is used because many problems arising in practice are *stiff*, for which the use of an explicit scheme requires impractically small time steps dt to keep the numerical integration within a desired accuracy.

Decisions Regarding the Integration Scheme

As has been discussed, the implicit scheme is typically stable for much longer time steps than the explicit scheme and often this means that the implicit scheme takes much less computational time. With that being said, whether one should use an explicit or implicit method depends upon the problem to be solved.

For an S-lay pipeline installation model, OrcaFlex requires an extremely small time step of around 0.00053 second to solve the equation of motions of the system. This is attributed to the non-linearity in the suspended pipeline geometry and also the quadratic drag term in the hydrodynamic forces. While the implicit integration scheme is stable with 0.1 second time step. Therefore, the implicit scheme is used for all simulations considered in this thesis.

2.5. Quantification Method and Statistical Definitions

This section explains the methodology used for comparing two signals and definition of the statistical parameters used to quantify the deviation between the two signals is given.

For model validation, the pipeline top tension is considered as the comparison parameter as the top tension during offshore installation is measured. Therefore, comparison with the real condition can be made. Additionally, tension is a parameter that governs the behaviour of the suspended pipeline, which means that the pipeline integrity can be ensured by maintaining the tension, specifically the extreme values of the tension is correlated with the extremes in strains and fatigue damage.

For this reason, instead of comparing the whole time history, the tension output from OrcaFlex model is validated with measurement by comparing the tension maxima and minima.

2.5.1. Tension Peak Detection

The maxima and minima from the model and measured tension signals are detected separately to prevent upon comparing maxima with minima. The explanation below will be given for maxima detection only since the procedure for minima is identical.

First, the built-in Matlab function *findpeaks* is used to detect all the maxima from the signal. The signal is basically stored as a discrete value in a vector. The *findpeaks* function define maxima as a data sample which is larger than the two neighbouring samples. The output of this function is positions and values of the detected peaks in the vector. Based on this output, the magnitude and time of occurrence of the maxima are known.

Since the extremes in tension are correlated with the extremes in the pipeline dynamics, a threshold with a value of 10% variation from the set tension is used to guarantee the peak detection to only detect the tension extremes, as they are correlated with the extremes pipeline dynamics.

The peak detection is done for both tension signals from OrcaFlex model and offshore measurement during 3-hour simulation. Visually, a snapshot of the peak detection is illustrated in Figure 2.24 below.

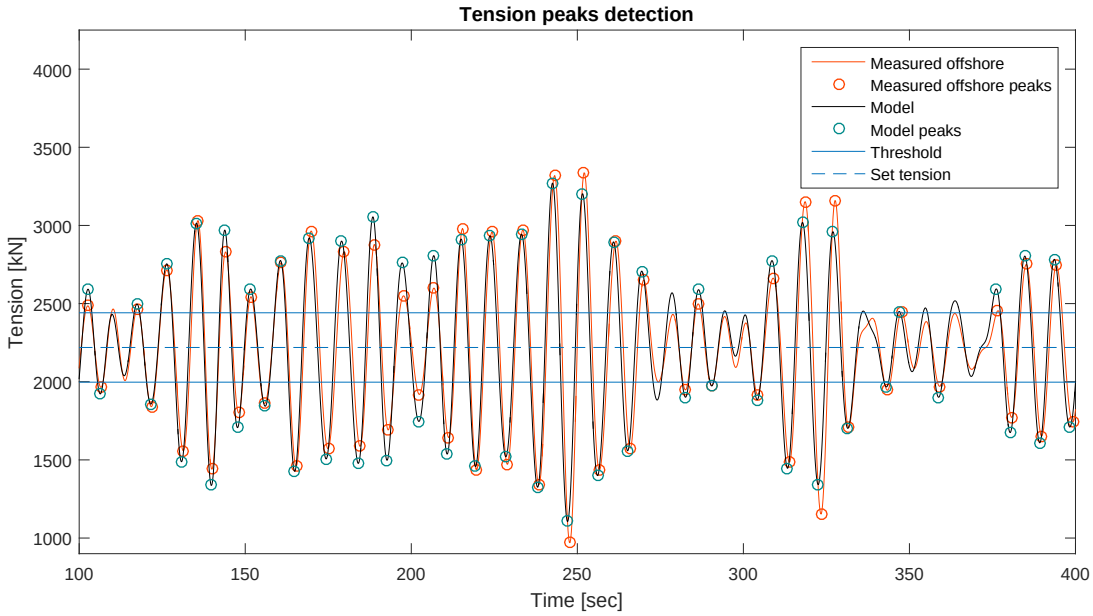

Figure 2.24: Tension peaks detection

2.5.2. Statistical Parameters

Once the tension tension maxima and minima from both signals are obtained, the next step is to compare these tension peaks by calculating the absolute and relative deviation of the model signal from measurement.

Absolute deviation and relative deviation are defined as follows,

$$\text{Absoulte deviation} = T_{model} - T_{measured} \tag{2.20}$$

$$\text{Relative deviation} = \frac{\text{Absolute deviation}}{\text{set tension} + |T_{measured} - \text{set tension}|} \tag{2.21}$$

Where T_{model} is the model tension peak and $T_{measured}$ is the measured tension peak. The comparison is done separately for the maxima and minima and the number of comparison is based on the number of available measured tension peaks. For each measured tension maxima, the algorithm finds the corresponding maxima from the model tension, which is the model tension maxima with the closest time of occurrence with the measured tension.

3

Model Validation and Sensitivity Study

In this chapter, the model validation for all case studies introduced in Chapter 2 is presented. OrcaFlex model is validated by comparing the output pipeline top tension to the measured tension during offshore installation. Section 3.1 discusses the results of tension comparison based on the distribution of tension relative deviations. Subsequently, section 3.2 provides the sensitivity study of several parameters which are influential to tension fluctuation. Based on the study results, recommendation for additional measurement to make a more realistic model is given.

3.1. Model Validation

Model validation is done by comparing the pipeline top tension output of OrcaFlex model to the offshore measured tension. As discussed in Section 2.4.4, prior to modelling the PI controller that governs the tensioner pay-out motion, the measured tensioner motions is specified to simulate the real tensioner behaviour. Schematically, the process is illustrated in Figure 3.1 below.

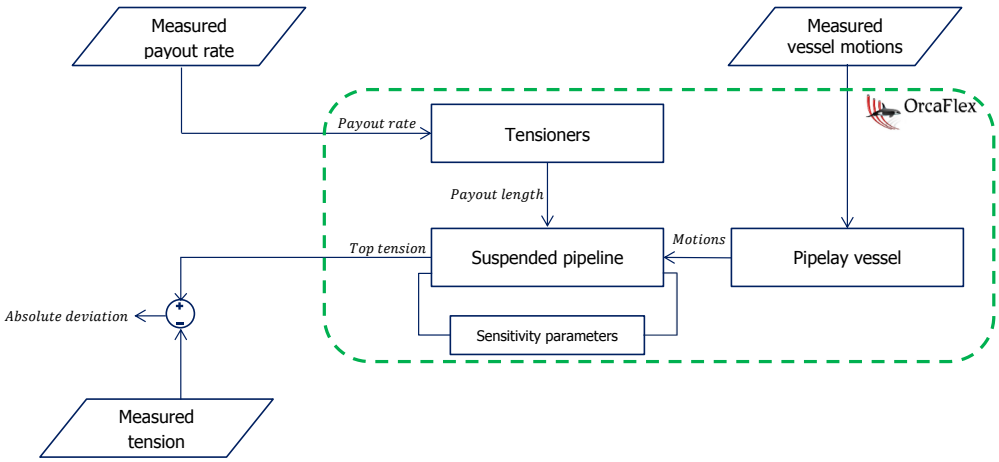

Figure 3.1: Schematic of model optimization

Subsequently, the statistical parameters introduced in Section 2.5.2 are used to quantify the deviation of the output pipeline top tension from offshore measured tension.

Overview of the relative deviation for all installation cases is shown in Figure 3.2. Positive relative deviations belong to model tension peaks which are larger than the corresponding measured tension peak and vice versa. In the first column, snapshots of the two tension signals are given. In the second and third column is the distribution of the relative deviations for tension maxima and minima respectively. Each distribution is computed from 3-hour simulation tension time history.

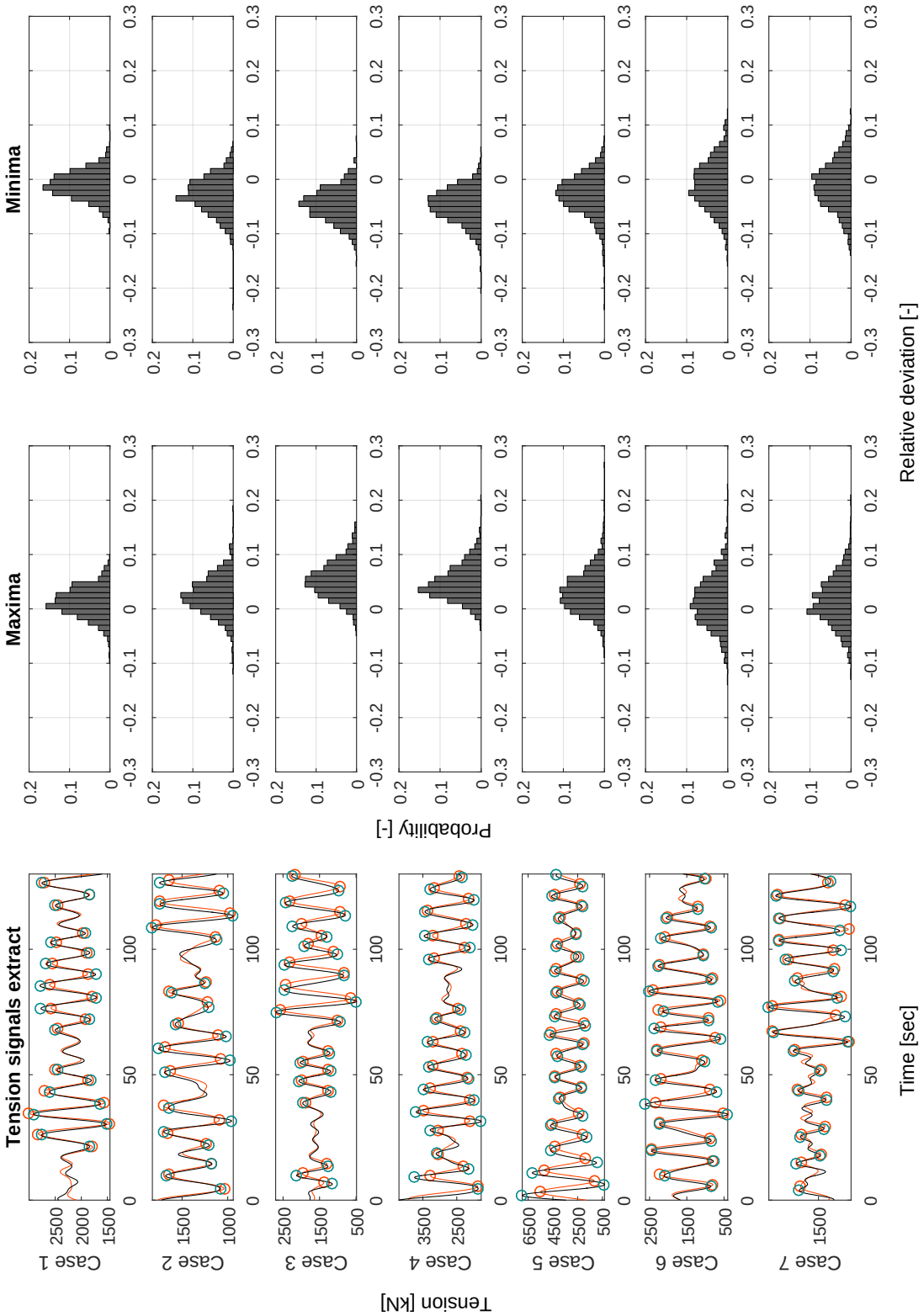

Figure 3.2: Initial results of relative deviation

Table 3.1 below gives the details of the relative deviation distribution shown in Figure 3.2. As the standard deviation becomes larger and the peak becomes lower, it can be seen that the tension relative deviation tend to increases as the water depth increases.

Table 3.1: Maximum, mean and minimum value of relative deviation

Case	Maxima				Minima			
	min.	mean	max.	St. dev.	min.	mean	max.	St. dev.
1	-0.09	0.01	0.09	0.03	-0.10	-0.01	0.09	0.02
2	-0.11	0.02	0.19	0.03	-0.23	-0.03	0.06	0.03
3	-0.05	0.05	0.16	0.03	-0.15	-0.05	0.07	0.03
4	-0.04	0.05	0.21	0.03	-0.21	-0.05	0.05	0.03
5	-0.09	0.03	0.27	0.04	-0.23	-0.03	0.07	0.04
6	-0.13	0.01	0.23	0.04	-0.15	-0.01	0.12	0.04
7	-0.13	0.01	0.21	0.04	-0.13	-0.01	0.13	0.04

It is also likely for the cases with concrete coating (Case 1 to Case 5) to have higher tension maxima and lower tension minima than the measured tension. This means that the model tension fluctuates more than the measured tension. On the other hand, Case 6 and 7, which are the case without concrete coating show similar fluctuation to the measured tension, with symmetrical maxima and minima distributions centred around zero.

Based on the installation characteristics given in Table 2.2, Case 6 is comparable with Case 5 as the vessel motions and water depths are identical. However, the tension in Case 5 fluctuates more than the measured tension compared to Case 6. Based on this, it is expected that the concrete coating plays a role in the symmetry of the dynamic tension. Concrete coating is modelled as weight to the pipeline and does not contributes to the structural stiffness. Therefore, influence of pipeline mass in this case expressed as the concrete coating density on dynamic tension fluctuation will be discussed in the next section.

3.2. Sensitivity Study

Based on the result in Section 3.1, sensitivity analysis is performed to investigate several parameters which are influential to the dynamic tension. Besides the concrete coating density, influence of set tension and current is also investigated.

As has been explained in Section 2.4.7, the static configuration is determined based on the average of the measured tension without subsea current presents. However, subsea current can cause appreciable static and dynamic load on the pipeline. The loads caused by current load occurs on regular basis (quasi-static) as the change of current period (e.g tide periods of approximately 12.5 hours) are essentially greater than fluctuation period of the pipeline motions.

At the same time, the pipe relative velocity to the fluid will also changes as the relative velocity will be greater for pipe motions in the same direction as the current direction, thus resulting in larger hydrodynamic force. While for the other half of oscillation period, the pipe oscillation counteracts the current direction, thus the hydrodynamic forces acting on the pipeline will be smaller.

Besides these parameters, sensitivity study of parameters which are expected to be insensitive to the tension fluctuation is checked to validate the assumption used in this thesis. In summary, sensitivity study will be performed for the pipe mass, set tension, current load, added mass coefficient, drag coefficient, wave-induced hydrodynamic force, and soil shear strength of the seabed. Firstly, the effects of each parameter on dynamic tension will be discussed. Then, a conclusion will be drawn based on the results.

3.2.1. Set Tension and Current Loads

Initially, the set tension is determined based on the mean of the measured tension signal. Therefore, it is expected that the maxima and minima are symmetrical around this value. However, this might not be the case if there is current load present, where the average of the tension signal is shifted towards either the maxima or the minima, depends on the current direction. Therefore, set tension could be one of the parameters which leads to uncertainty in the static configuration.

Firstly, sensitivity of the set tension is intended to investigate the influence set tension on the dynamic tension. Subsequently, current sensitivity analysis is performed by varying the flow directions. To model a

realistic current profile, an exponentially distributed current velocity is used. It is described mathematically by the following equation:

$$S = S_b + (S_f - S_b) \cdot \left(\frac{Z - Z_b}{Z_f - Z_b} \right)^{1/\alpha} \tag{3.1}$$

Where S_f and S_b are the current speeds at the sea surface and seabed, respectively, Z_f is the water surface Z level, in this case is zero and Z_b is the Z level of the seabed, α is the power law exponent which determines the decaying profile, typically $\alpha = 7$. With a smaller α, the decay is spread more evenly across the water depth. With a higher value, the decay mostly occurs close to the seabed. Current speed of 1m/s at the sea surface is chosen as it is expected as a large magnitude of current load during installation. The current profile is illustrated in Figure 3.3a below.

Since different current direction has different effects on tension fluctuation, five possible current directions that might happened during offshore installation are considered, start from 0 deg to 180 deg with 45 deg direction step as shown in Figure 3.3b. The other half of the possible current directions is assumed to have the same influence as the pipelay configuration is symmetrical.

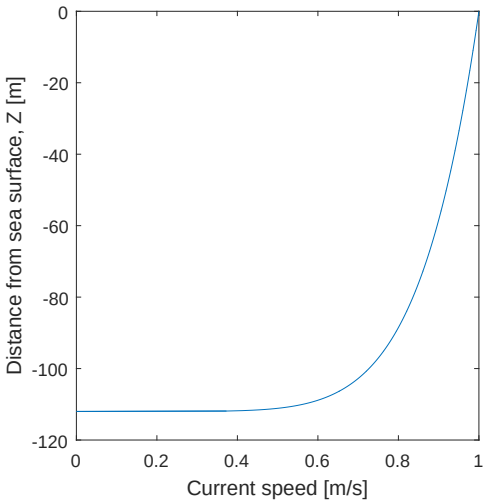

(a) Current profile

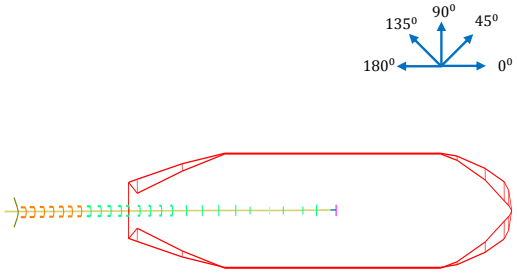

(b) Current direction

Figure 3.3: Current load profile and direction used for sensitivity analysis

In order to present a representative value of the tension fluctuation, the fluctuation is described by a maximum and minimum tension for a given tension signal. The maximum and minimum are calculated as the mean of the tension data with probability of exceedance of 90 %. Therefore, the maximum is mean of the top 10 % of the highest data and the minimum is mean of the top 10% of the lowest data.

Shallow water: Case 1

Since the assumption of using the mean of the measured tension signal as set tension might not valid if significant current load is present, the influence of set tension on tension fluctuation is investigated. Several models with different set tension are considered and the influence on tension fluctuation is examined.

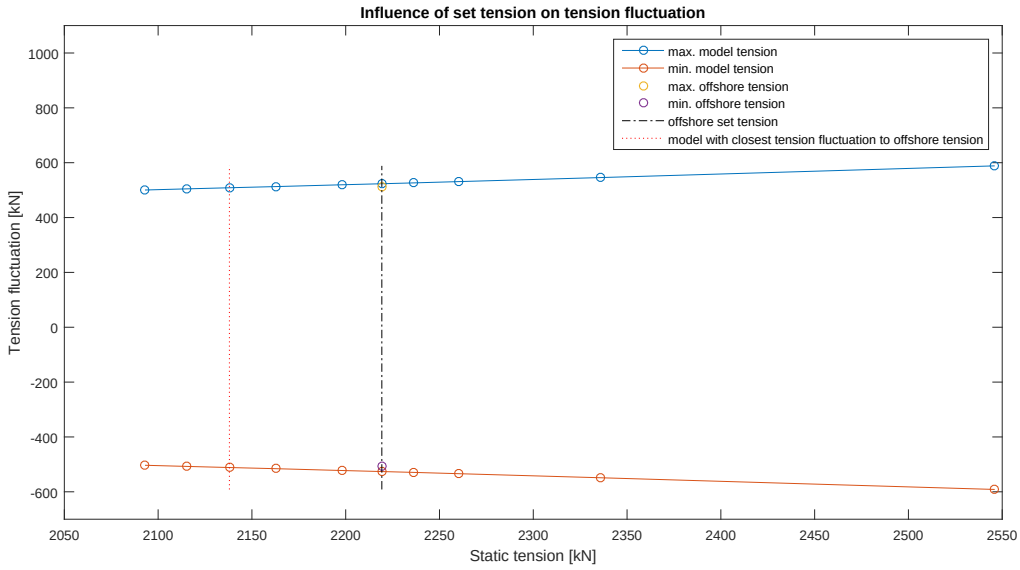

Figure 3.4: Influence of set tension on dynamic tension fluctuation in shallow water

It can be seen in Figure 3.4 that set tension is proportional to the tension fluctuation. A higher set tension applied to the model results in larger tension fluctuation, and vice versa. By varying the set tension, it is found that the model with reduced set tension to 2138 kN gives the closest tension fluctuation to the offshore measured tension.

Subsequently, current load sensitivity analysis is performed based on the model with reduced set tension to emphasise the effect of current load on set tension. Figure 3.5 shows that current in the 0 deg and 180 deg are the most influential to mean tension signal.

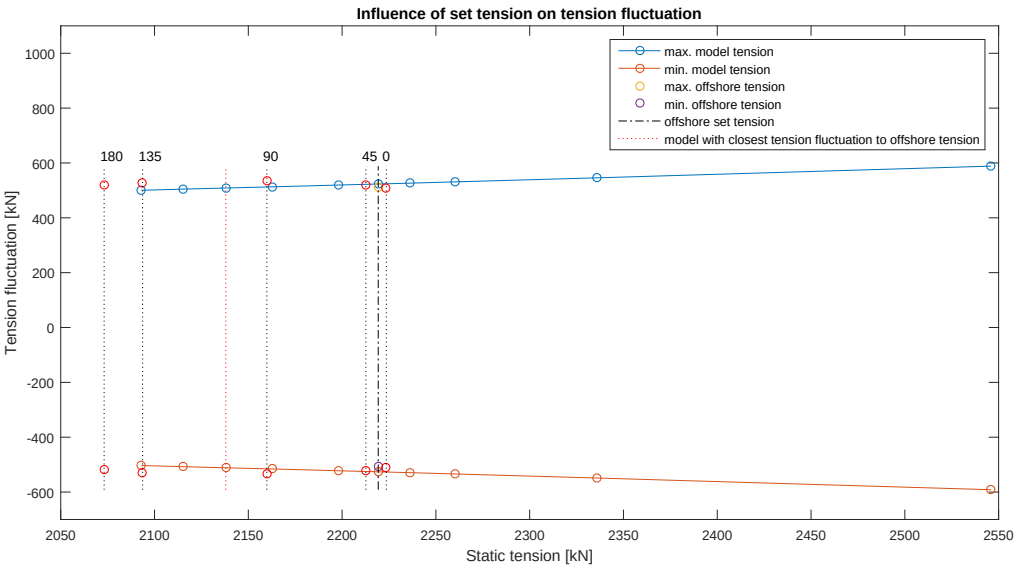

Figure 3.5: Influence of current direction on pipeline top tension

In OrcaFlex, the current force acting on the pipe are calculated by using the *cross flow* principle, where the fluid velocity relative to the pipe is split into the normal and axial components. The drag force due to current for each component is calculated based on the drag term in Morison equation as expressed in Equation 2.1.

The presence of current in the 0 deg and 180 deg direction are the most influential as shift in mean tension is at the largest in these two directions. Due to the configuration of the suspended pipeline, current in the 180 deg direction generates force in the upward direction which counteracts the pipeline weight thus lower the mean tension. On the other hand, current in the 0 deg direction generates force in the downward direction which is in the same direction as pipeline weight thus results in larger mean tension. Besides the effect on mean tension, it is also observed that the current load has little influence on the tension fluctuation.

Deep water: Case 5

In the deep water case, the change in set tension is more influential to the tension fluctuation as can be seen in Figure 3.6. This is due to the change in pipeline length required to change the same amount of set tension is much larger in deep water case. Due to this larger change in the suspended pipeline span and configuration, the change in system stiffness and mass is therefore more significant thus the change in dynamic response is more obvious.

It can be observed in Figure 3.6 that current load has more influence in the deep water case as the mean tension is shifted more than in the shallow water case. This can be attributed to the longer suspended pipeline length thus the accumulated hydrodynamic force acting along the pipeline becomes larger.

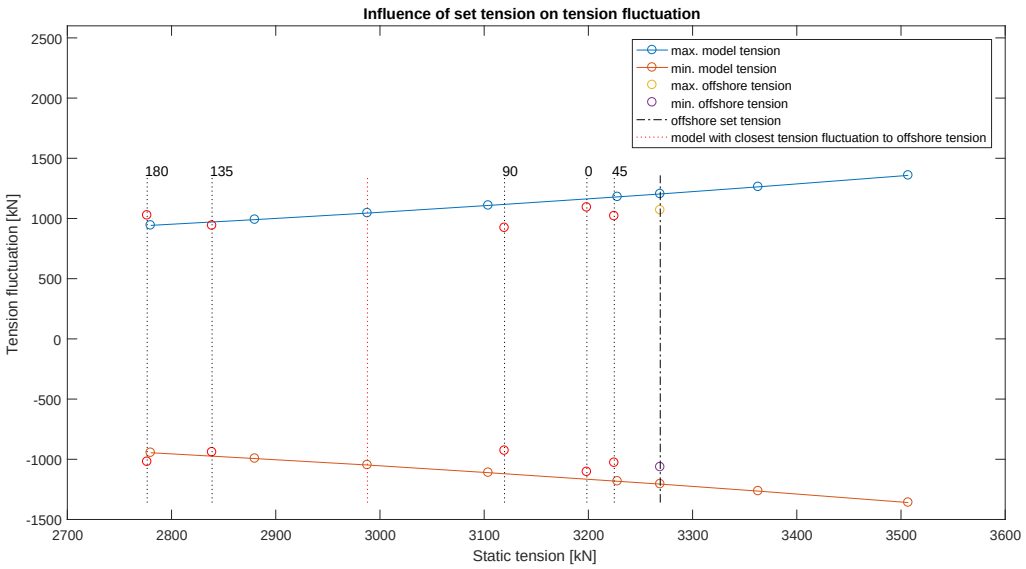

Figure 3.6: Influence of set tension on dynamic tension fluctuation in deep water

However, the most significant current direction is in the 45 deg direction, which can be decomposed into current components in 0 deg and 90 deg direction. The 0 deg component contributes to the force acting in the same direction as gravitational force, as has been explained in shallow water case. While in the 90 deg direction, the catenary stiffness is at the lowest compared to the other direction, which means that the pipeline will be displaced at the most due to current in this direction.

Besides the shift, current with a component in the lateral direction dampen the dynamic tension as can be seen in the model with current direction of 90 deg, 135 deg and 45 deg. This is due to the pipe oscillation velocity in deep water is not as high as in shallow water. Therefore, with a current speed of 1m/s the relative velocity will increase quite significantly, which gives significant increase in the drag component of the pipeline hydrodynamic force.

3.2.2. Concrete Coating Density

As mentioned in Section 3.1, concrete coating density might explain the overestimation of the measured tension fluctuation by the model. Uncertainty in concrete coating density might be caused by the aggregate composition and water absorbed in the concrete pore space. Influence of concrete coating density on dynamic tension is discussed in the following section. Sensitivity of concrete coating density is performed in the absence of current load.

Shallow water: Case 1

The sensitivity analysis is done by increasing the concrete coating density from its initial value. Based on the result shown in Figure 3.7, the tension fluctuation is reduced as concrete coating density increases and at a value of 4% increase, the model tension fluctuation is at the closest to the measured tension fluctuation.

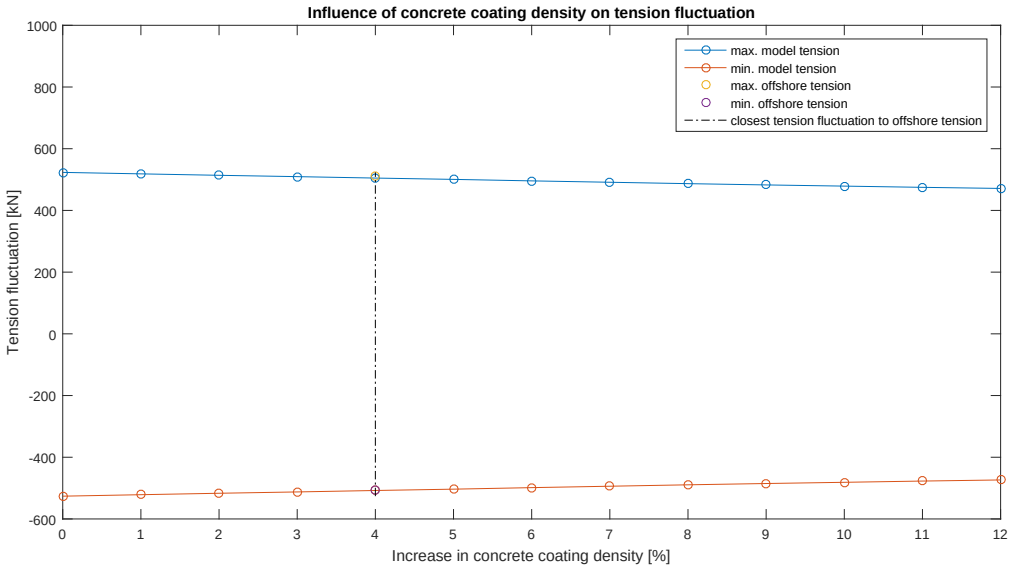

Figure 3.7: Concrete coating density sensitivity

Besides the tension fluctuation, increase in concrete coating density will also affects the stinger tip clearance. Stinger tip clearance is maintained during installation so that the pipeline does not have contact with the stinger tip as this is also one of the installation criteria in S-lay mode. The influence of increase in concrete coating density on stinger tip clearance is shown in Figure 3.8.

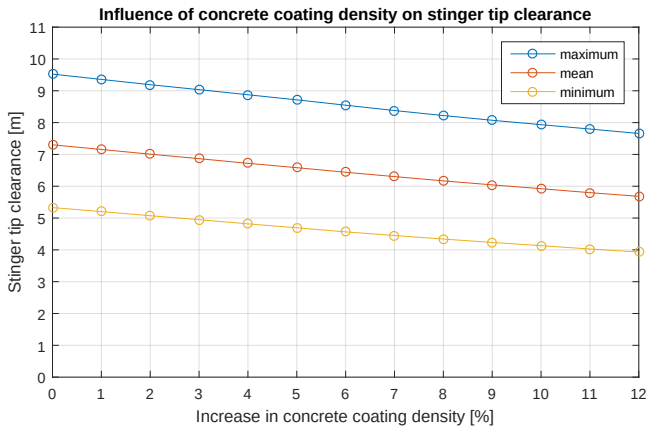

Figure 3.8: Range graph of stinger tip clearance for different increase in concrete coating density

It can be seen in Figure 3.8 that the clearance is still large even with a very heavy pipe. This is attributed to the shape of the suspended pipeline in shallow water is more straight compare to the deep water thus the stinger tip clearance is large.

Deep water: Case 5

In the deep water, the influence of the increase in concrete coating density is more significant due to the longer suspended pipeline span. Result of the sensitivity is shown in Figure 3.9. Similar to Case 1 in shallow water, 4% increase in concrete coating density leads to the most similar tension fluctuation to the measured tension fluctuation.

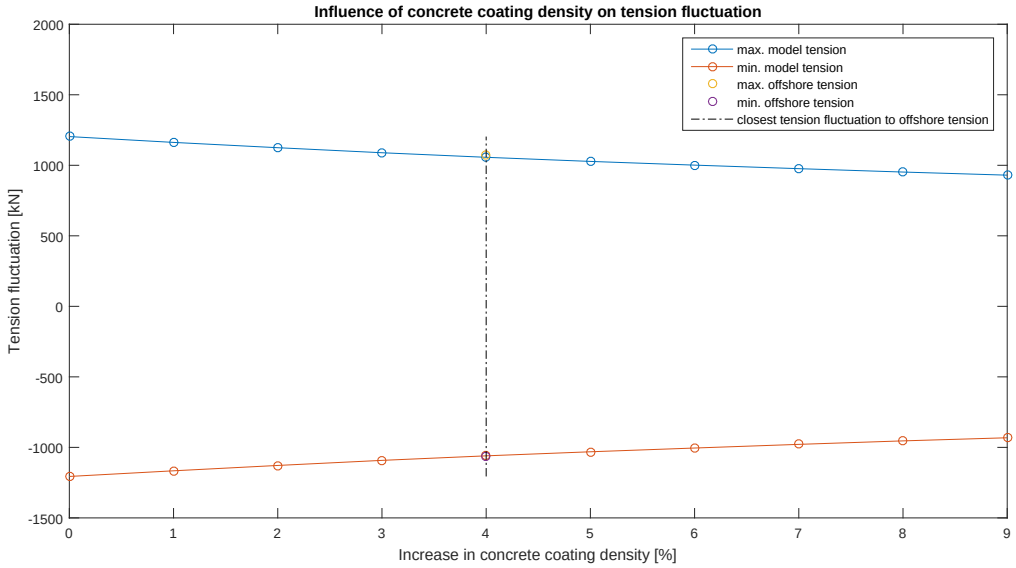

Figure 3.9: Concrete coating density sensitivity

The stinger tip clearance in deep water is lower due to the inherent static configuration in deep water. It can be seen that stinger tip contact occurs starting from 9% increase in concrete coating density. However, with the optimized value of 4% increase, the pipeline still have no contact with the stinger tip.

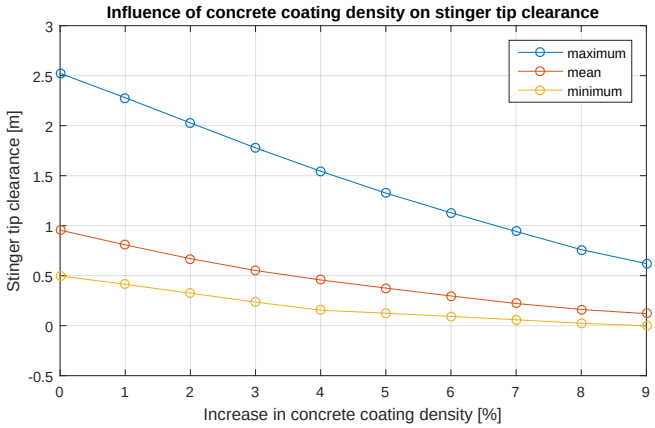

Figure 3.10: Range graph of stinger tip clearance for different increase in concrete coating density

Overview of all cases

Since the two cases above give identical result, the other cases are investigated to check whether the increase in concrete coating density is identical for all cases. Overview of the concrete coating density which

gives the closest tension fluctuation to the measured tension can be seen in Appendix A.5. Based on the results, it can be concluded that optimization of concrete coating density alone would not lead to a converged value of concrete coating density that can be used for predictive study. However, the uncertainty in concrete coating density might explain a large part of the tension overestimation.

3.2.3. Pipeline Added Mass Coefficient

Pipeline added mass coefficient is determined based on the KC-number variations as discussed in Section 2.4.6. In this section, the influence of the added mass coefficient on tension fluctuation is discussed. It can be seen in Figure 3.11 and 3.12 that the added mass coefficient is proportional to the dynamic tension fluctuation. This is due to the added mass coefficient is proportional to the inertia force which is part of the hydrodynamic force acting on the pipeline.

It is also observed that the added mass coefficient becomes more influential in the deep water case as increase in tension fluctuation becomes larger with increasing added mass coefficient. This is due the length of suspended pipeline span which interacts with fluid is longer in the deep water case.

Shallow water: Case 1

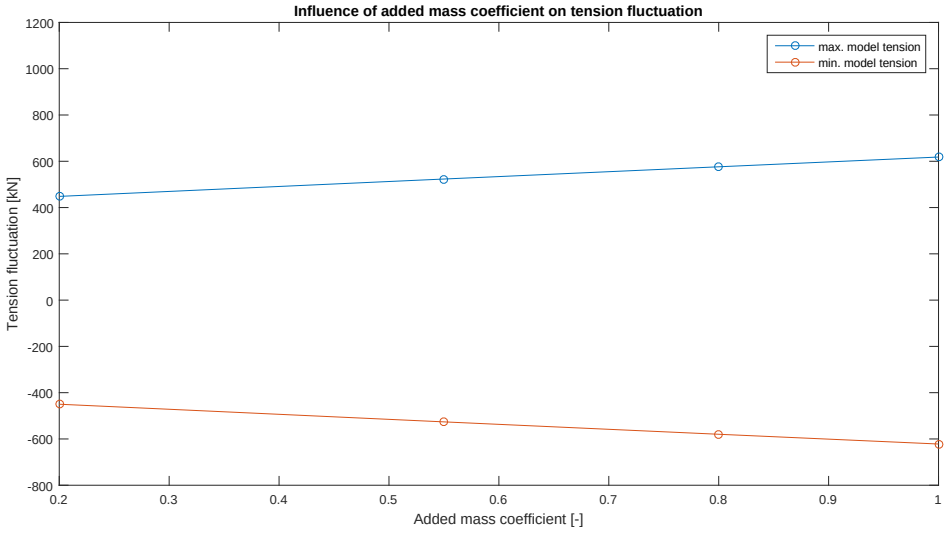

Figure 3.11: Influence of added mass coefficient on tension fluctuation in shallow water case

Deep water: Case 5

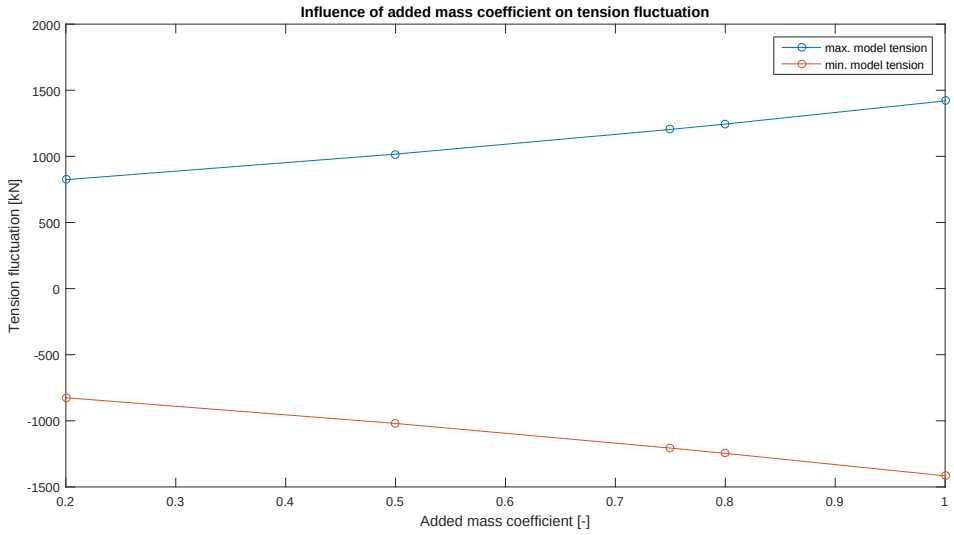

Figure 3.12: Influence of added mass coefficient on tension fluctuation in shallow water case

3.2.4. Pipeline Drag Coefficient

As mentioned in Chapter 2, pipeline drag coefficient depends on the Reynolds number. First, it is investigated whether it is necessary to implement the drag coefficient as a function of Reynolds number or a simplified method with a constant drag coefficient is sufficient. Two models are introduced: model with drag coefficient as a function of Reynolds number and model with a constant drag coefficient at the maximum value of 1.2.

Absolute deviation is calculated as the deviation of tension peaks from model with variable drag coefficient from model tension peak of model with a constant drag coefficient. Distribution of the relative deviations is shown in Figure 3.13 and Figure 3.13. Since the relative deviations are relatively low with the maximum tension relative deviation of 3%, it is concluded that the drag coefficients can be evaluated at the maximum value of drag coefficient, and thus becoming time independent.

Shallow water: Case 1

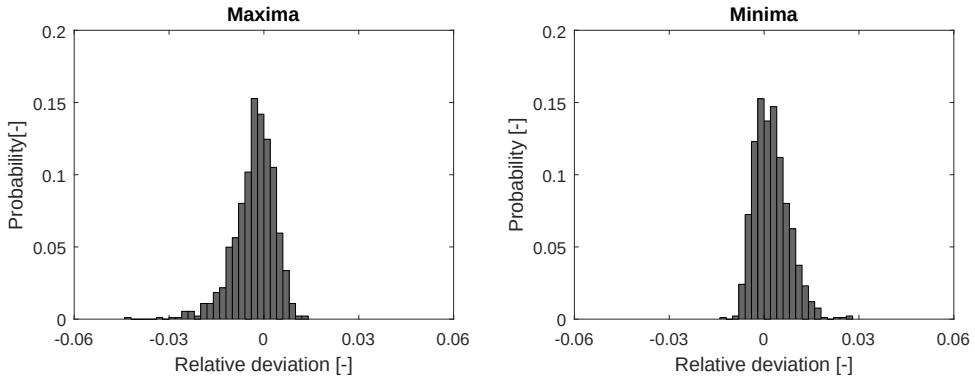

Figure 3.13: Shallow water case : distribution of tension peak relative deviations of model with constant drag coefficient of 1.2 and model with Reynolds number-dependent drag coefficient

Deep water: Case 5

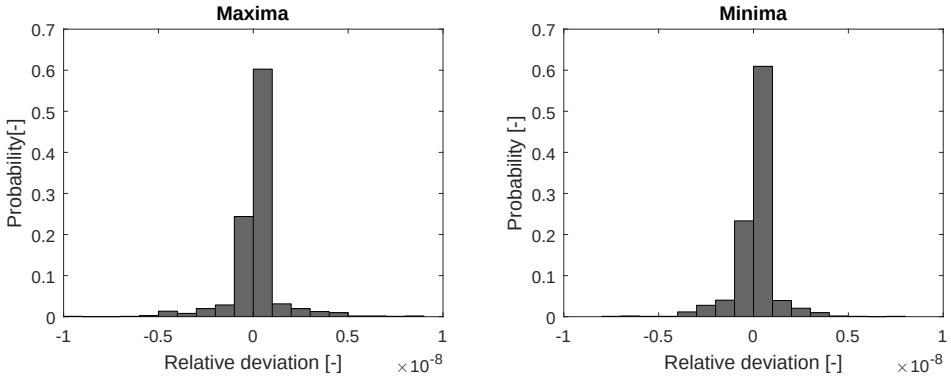

Figure 3.14: Deep water case : distribution of tension peak relative deviations of model with a constant drag coefficient of 1.2 and model with Reynolds number-dependent drag coefficient

3.2.5. Wave-Induced Hydrodynamic Force on Pipeline

In this case, the significance of the wave induced force on pipeline top tension is investigated. The vessel motions are calculated by using the Response Amplitude Operator (RAO) with a specified JONSWAP spectrum of the wave. The output vessel motions time history from the 3-hour simulation are then extracted and used as input for a comparison model. Five wave directions are considered for both shallow water case and deep water case as shown in Figure 3.15. For each direction, the resulting vessel motions are extracted and are used as input for the vessel motions of the model with still water.

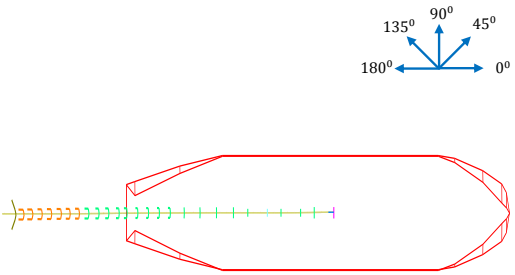

Figure 3.15: Wave directions

Subsequently, the tension output of these two models are compared to investigate whether the wave-induced force is negligible or not. Based on the result shown in Figure 3.16 and 3.17, it can be seen that the most influential wave direction is in the 45 deg direction as the maximum relative deviation is at the largest among all considered directions. However, the influence of the wave-induced force on the pipeline top tension is relatively small thus can be neglected. Moreover, in the deep water case, tension relative deviation become smaller due to the decaying profile of the water particle kinematics as a function of vertical distance from the wave surface. For this reason, the influence of the wave force in the lower span of the suspended pipeline is insignificant thus the difference in pipeline top tension with the model where vessel motions are used as inputs becomes smaller. Therefore, the assumption used in this thesis of using the measured vessel motions as inputs to the model is valid.

Shallow water: Case 1

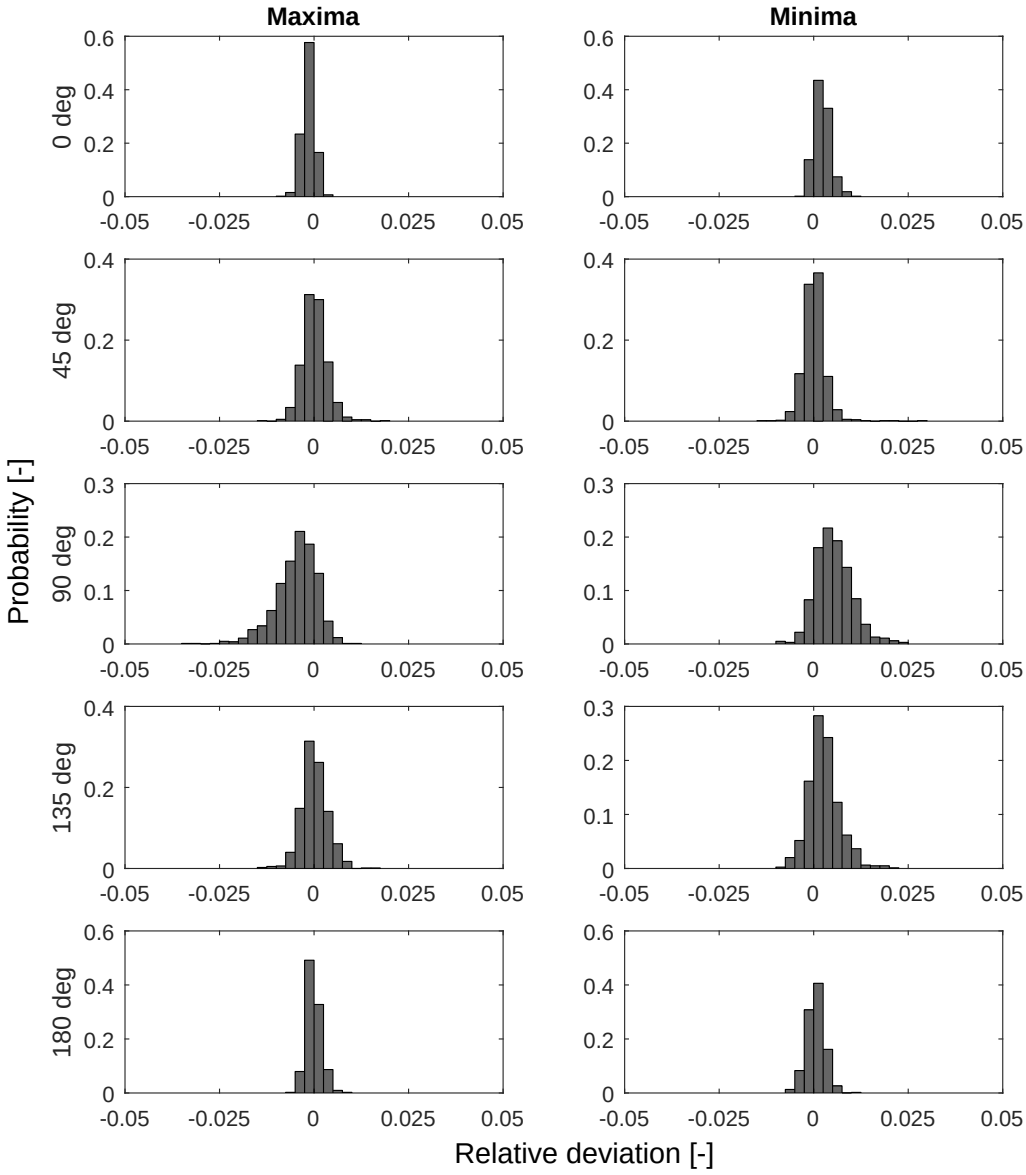

Figure 3.16: Shallow water case : distribution of tension peak relative deviations of model with included wave force from model with input vessel motions

Deep water: Case 5

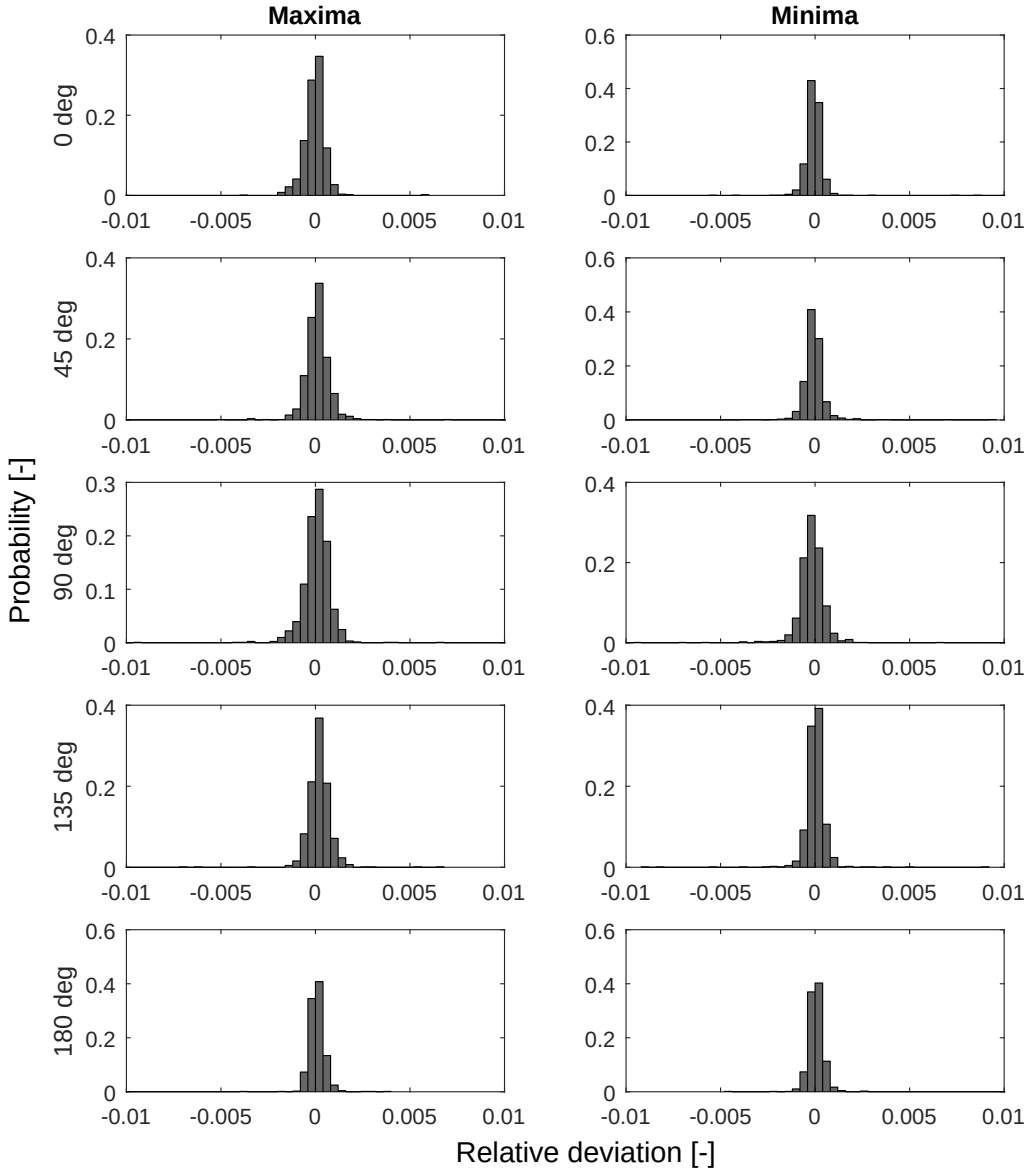

Figure 3.17: Deep water case : distribution of tension peak relative deviations of model with included wave force from model with input vessel motions

3.2.6. Soil Shear Strength of the Seabed

Seabed model is characterised by the undrained shear strength of the soil. However, soil investigation result is not always available at the exact location of each case study. Therefore, shear strength for each case study is determined based on the soil properties at the closest location where geotechnical investigation is available. Moreover, the soil properties might be varying along the pipeline span on the seabed. Therefore, sensitivity analysis for the soil shear strength is performed.

Three additional models with different undrained shear strength, c_u are considered. The undrained shear strength from the geotechnical investigation is found to be around one as given in Table 2.3. For the additional models, it is increased up to 12 and then, the tension relative deviation is calculated to investigate the sensitivity. Based on the results shown in Figure 3.18 and Figure 3.19, it is observed that the increase in soil shear strength results in lower tension fluctuation, this can be seen more obviously in the shallow water case, shown by Figure 3.18. However, the effect of different soil characteristics is negligible thus the model with the assumption of soil characteristics taken from the nearest investigation location is valid.

Shallow water: Case 1

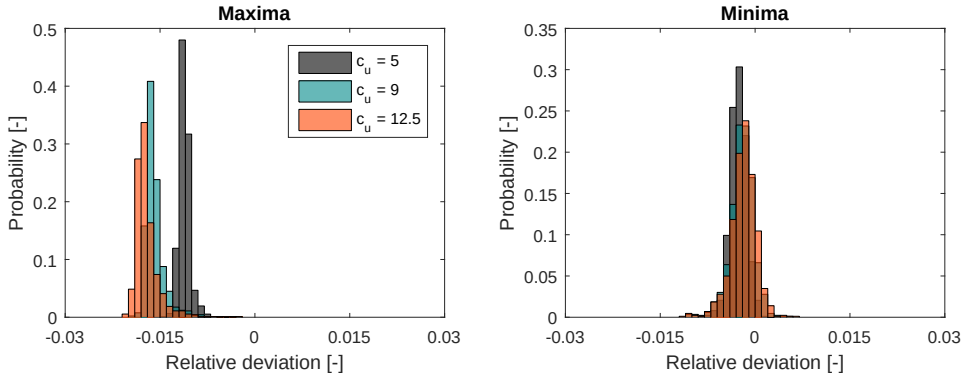

Figure 3.18: Shallow water case : distribution of tension peak relative deviations of model with different soil shear strength form model with shear strength from data

Deep water: Case 5

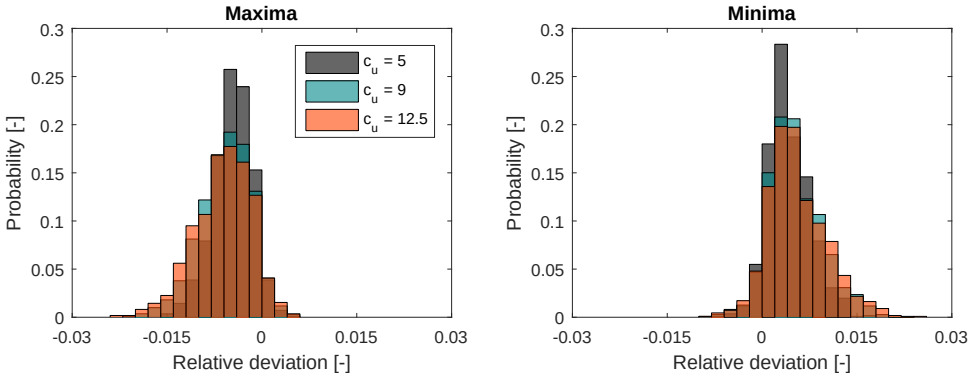

Figure 3.19: Deep water case : distribution of tension peak relative deviations of model with different soil shear strength form model with shear strength from data

3.3. Chapter Conclusion

Measured tension fluctuation is overestimated by the model for cases with the concrete coated pipeline. Based on the sensitivity study, there are several parameters which are found to be influential and might be attributed to the larger tension fluctuation by the model. It is found that heavier pipeline results in less dynamic tension fluctuation, which is shown by sensitivity analysis of the concrete coating density. Based on the sensitivity analysis, uncertainty in the concrete coating density might explain a large part in the symmetry of the relative deviation distribution. Uncertainty in concrete coating weight may be attributed to the water absorption, material compositions, and thickness of the concrete coating. However, optimisation of the concrete coating weight alone is not sufficient as it would not lead to a converged value that can be used for a predictive study.

Set tension of the model is assumed to be equal to the mean of measured tension. However, Section 3.2.1 shows that this assumption might not always be valid in the presence of current load with significant velocity as current loads affect both the static and dynamic of the tension signal. Also, it is found that the set tension is proportional to dynamic tension fluctuation. A higher set tension applied to the model results in larger tension fluctuations and vice versa, lower set tension results in lower tension fluctuation.

In shallow water, current acting in the 180 deg and 0 deg direction is the most significant to the shift in set tension. This is due to the vertical component of each current direction. For the 180 deg current direction, the vertical component counteracts the pipeline weight thus the set tension is lower. While in the 0 deg direction, the vertical component of the current acts in the same direction as the pipeline weight and thereby increases the set tension.

In deep water, besides 180 deg and 0 deg directions, current in the 90 deg direction is also significant to the change in set tension. This is due to the catenary stiffness of the suspended pipeline in this lateral direction is at the lowest, which means that the pipeline will be displaced at the most due to current flow in this direction. Therefore, it is found that the most significant current direction as combination of these two directions, which is in the 45 deg direction. Current in the lateral direction gives the most damping effect on the pipeline tension fluctuation. However, it also depends on the magnitude of the relative velocity between current and the pipeline.

Is is found that simplification can be made into the model. First, the pipeline drag coefficient can be implemented at the maximum operating value of 1.2 which results in a negligible difference compared to the Reynolds number dependent drag coefficient. Secondly, tension fluctuation induced by the wave force is found to be negligible compared to tension fluctuation induced by vessel motions thus the method used in this thesis of using the measured vessel motions as inputs are valid. Lastly, since the soil shear strength is insignificant to the pipeline top tension fluctuation, soil properties used in the seabed model can be determined based on the closest location where a soil investigation is available.

To obtain a more accurate model, it is recommended to measure the stinger tip clearance to validate the current load that is presence during offshore installation. Additionally, it is also recommended to do an experimental study which gives an accurate value of the concrete coating weight. For now, due to the unavailability of current measurements and information about the uncertainty in the concrete coating density. The initial models shown in Section 3.1 is considered as valid and thus will be used for subsequent analyses.

4

PI Controller Tuning and Comparisons with Simplified Controller Models

This chapter explains the tuning procedure of the PI controller model and subsequently, the influence of different tensioner models/modes to the pipeline integrity is given. Lastly, a conclusion about the reliability of the tensioner models that should be used for predictive study is given.

4.1. PI Controller

4.1.1. On-board Controller Gains

The PI controller gains of the tensioners on Solitaire is logged during offshore operations. These controller gains during the 3-hour period might be a constant value or time-variant, depends on the operator settings on the vessel. Overview of the gains of all case studies considered in this thesis is shown in Table 4.1 below.

Table 4.1: PI controller gains of the tensioners on board Solitaire

Controller gain	Case 1	Case 2	Case 3	Case 4	Case 5	Case 6	Case 7
Proportional [%]	88-120	140-160	90	85	85	96-106	84
Integral [%]	230	230-232	231	231	231	229-230	230

It can be seen that the settings for integral gains are likely to be around 231%. While the proportional gain seems to be the parameter to adjust by the operator.

4.1.2. PI Controller Model

Interaction between OrcaFlex and the PI controller model is schematically described in Figure 4.1 below. The controller gain is tuned to minimised the deviation from measured payout rate.

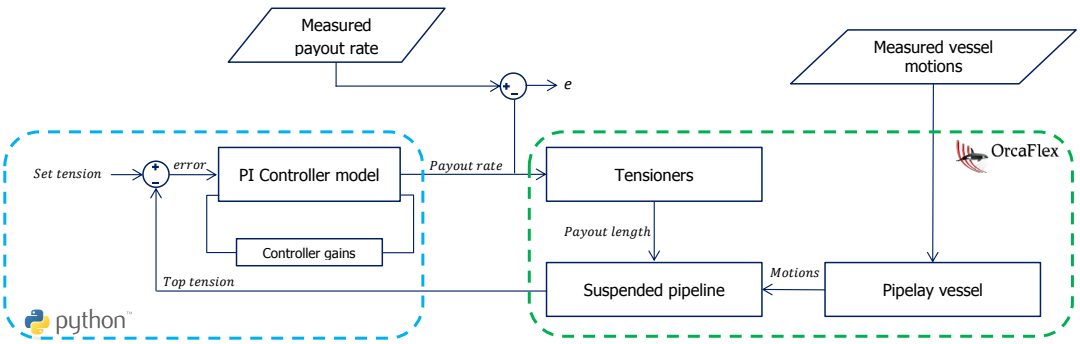

Figure 4.1: Procedure of PI controller tuning

Based on the logged controller gains, the ratio of $\theta = \frac{P_{gain}}{I_{gain}}$ is known. The same ratio can be used for controller gains of the model. Therefore, the tuning process of the PI controller model can be done by optimizing one of the gains only. While the other gain is determined based on the ratio θ. Integral gain is chosen as the tuning parameter as it tends to be constant in all case studies investigated in this thesis. Therefore, the same integral gain can be used for all case studies. While the proportional gain for each case is determined based on the θ value calculated from the logged controller gains in Table 4.1.

The controller gains are optimised based on Case 4. It is convenient to tune the controller gain based on this case as it has the longest period of tensioner payout without pulls. The controller gain combinations considered for the controller tuning are shown in Table 4.2 below. For each combination, the θ value is constant and equal to the θ from the logged controller gains of Case 4.

Table 4.2: Combination of P and I gains for controller tuning

P gain (%)	I gain (%)
0.00005	0.0001
0.00011	0.0003
0.00018	0.0005
0.00024	0.0007
0.00030	0.0008
0.00036	0.0010
0.00043	0.0012
0.00049	0.0013
0.00055	0.0015
0.00061	0.0017
0.00068	0.0018

The PI controller model is optimized to be able to reproduce the tensioner payout rate as measured. The optimization is done by considering the payout rate signal within the duration without pulls. This is done as during pulls, the vessel and the payout motions are not in stationary condition which is not modelled in OrcaFlex. The controller tuning result is shown by a cost function in Figure 4.2 below.

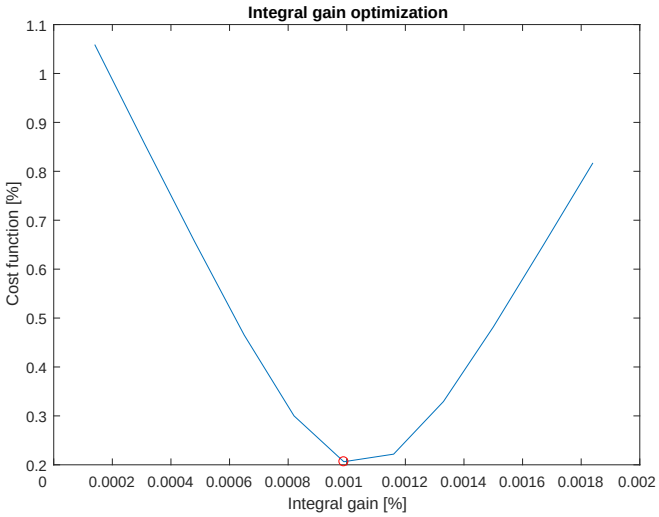

Figure 4.2: Cost function of PI controller gains optimization

It is found that the integral gain of 0.001% is the most optimum, which gives the closest approximation to the real tensioner payout rate. The time history of the two payout rate signals is presented in Figure 4.3.

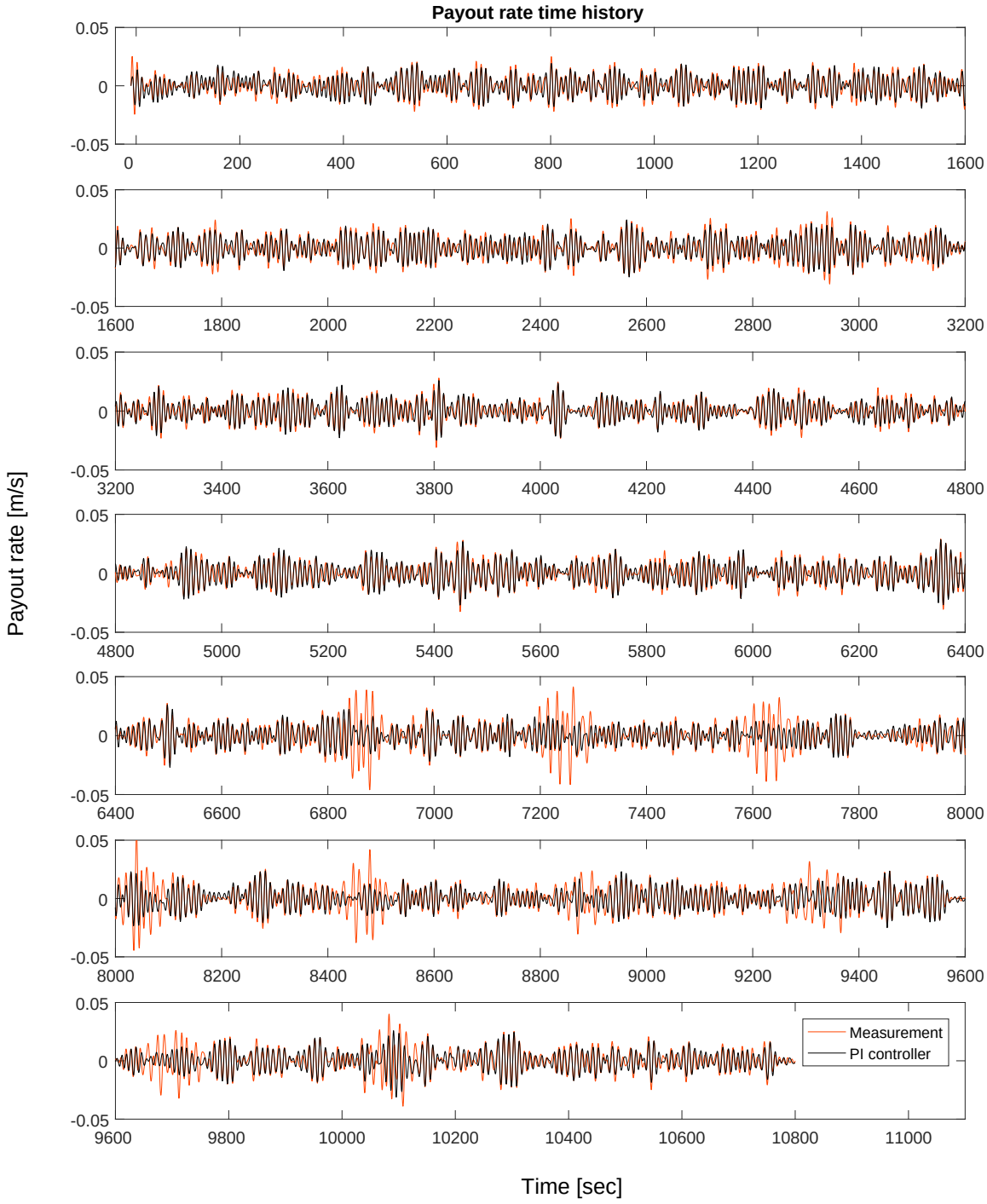

Figure 4.3: Payout rate time history

The PI controller model shows a good agreement with measurement during the period without pulls. However, relatively large deviations are observed during pulls, which can be seen within the period starting from simulation time of 6800 seconds, as shown in Figure 4.3.

Payout rate from the PI controller model shows less fluctuation than the measured payout rate during a pull. This is attributed to the vessel movement during pulls which is controlled by a Dynamic Positioning (DP) system. The DP system in Solitaire is controlled by a controller to adjust the thrust force required to move the vessel forward to the desired position, which means it is probable that the vessel exceeds the desired position thus the apply a corrective action until the desired position is achieved. During this adjustment period, the vessel is not in steady state condition, which generates larger payout rate by the tensioner to maintain the tension.

The integral controller gain for the other cases are set to be 0.001% as well, while the proportional gain is scaled linearly based on the logged controller gains. The absolute deviations as introduced in Section 2.5.2 are used to compare the payout rate signals and the distribution of the absolute deviation of payout rate peaks is shown in Figure 4.4. As the controller tuning is done only during the period without pulls, the absolute deviation is calculated for the signal segments without pulls.

Since the controller gains are optimized based on Case 4, it can be seen in Figure 4.4 that the absolute deviation distribution is symmetrical for Case 4, which means that the fluctuation of the payout rate are the same with the measured payout rate. However, the distribution is not always symmetrical for the other cases.

Despite the fact that there is a deviation in the measured payout rate signal, the influence of this deviation on pipeline top tension is negligible as the relative deviation between the tension signal peaks between the model with PI controller and model with specified payout rate are relatively small, with maximum relative deviation of less than 4 %, as shown in Figure 4.4.

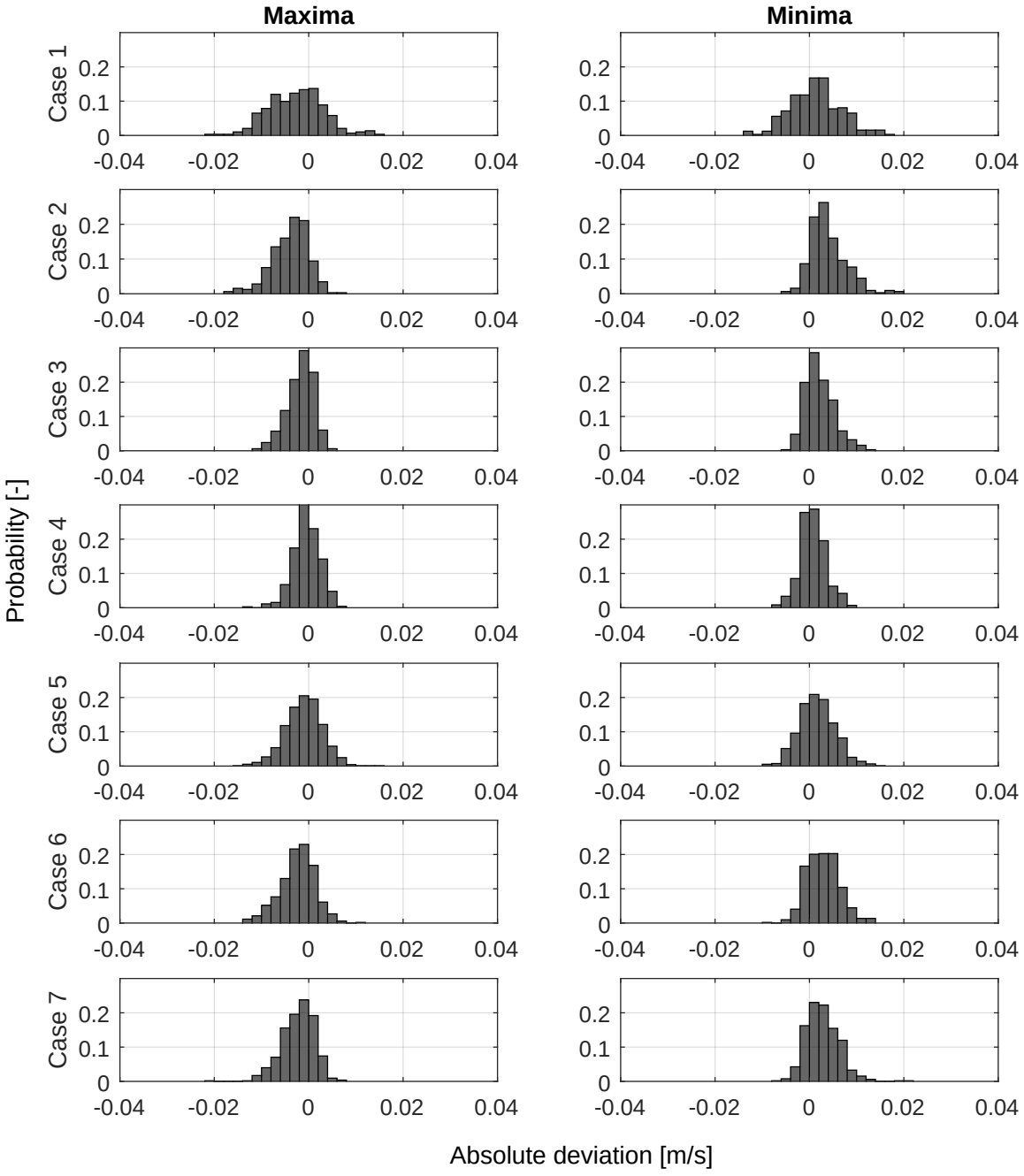

Figure 4.4: Distribution of the payout rate absolute deviation between the model with PI controller and model with input payout

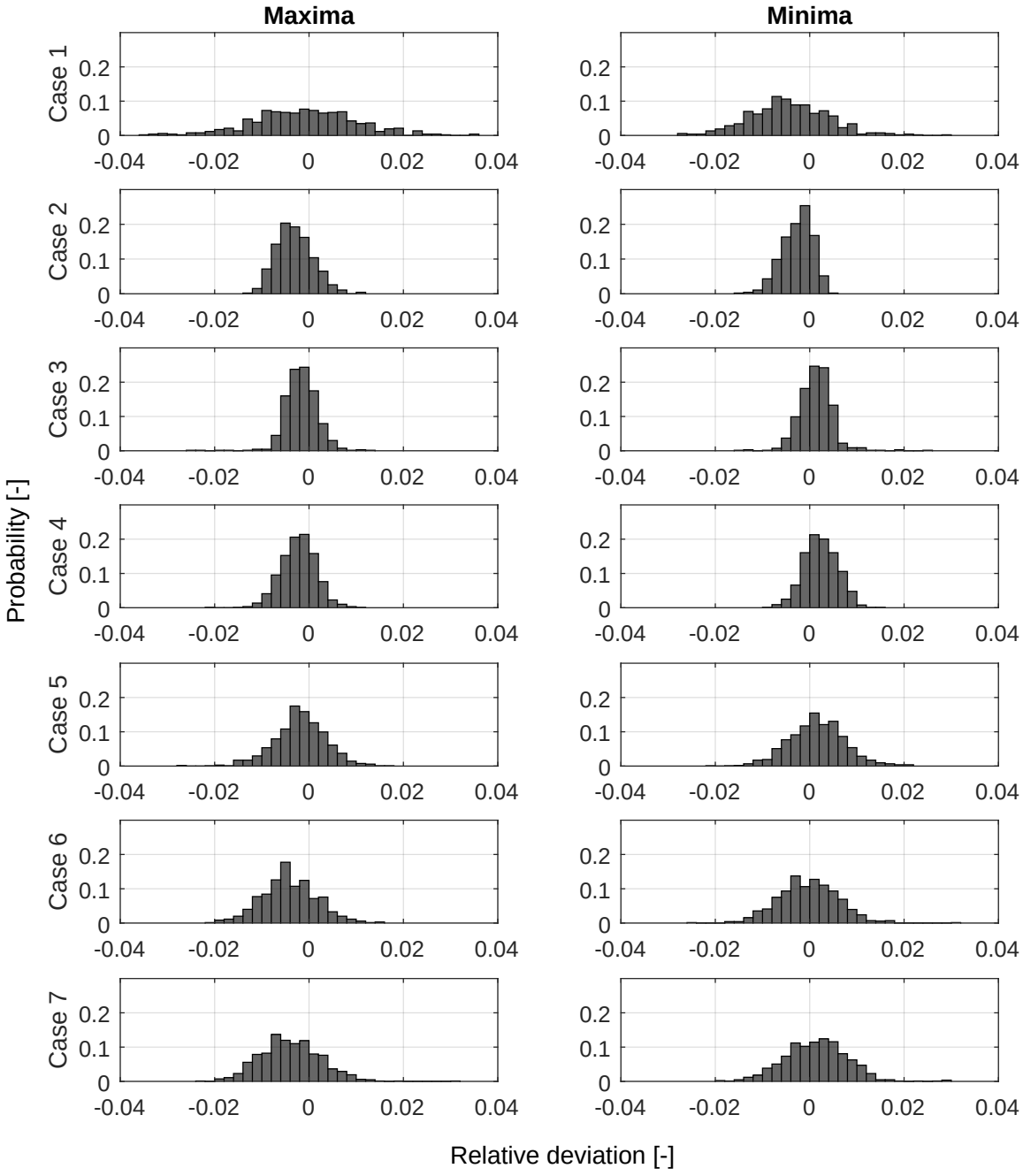

Figure 4.5: Distribution of the tension peak relative deviation between the model with PI controller and model with input payout

c

4.2. Pipeline Integrity Check

The curvature of the pipe span in the overbend follows the stinger curvature. Therefore, the dynamic behaviour is maintained. In contrast, dynamics in the sagbend are governed by the tension in the pipeline, which is influenced by the tensioner. Pipeline dynamics in the sagbend may harm the pipeline due to the amplification in maximum strain and accumulated fatigue damage. Therefore, different tensioner models will be compared and conclusions will be made based on the resulting pipeline integrity check expressed by the maximum von Mises strain and fatigue damage.

4.2.1. Maximum von Mises strain

Maximum von Mises strain resulting from models with different controller models are compared. The controller models which are used for comparisons are introduced in Chapter 2. The comparison of maximum von Mises strain in the sagbend for all cases is shown in Figure below.

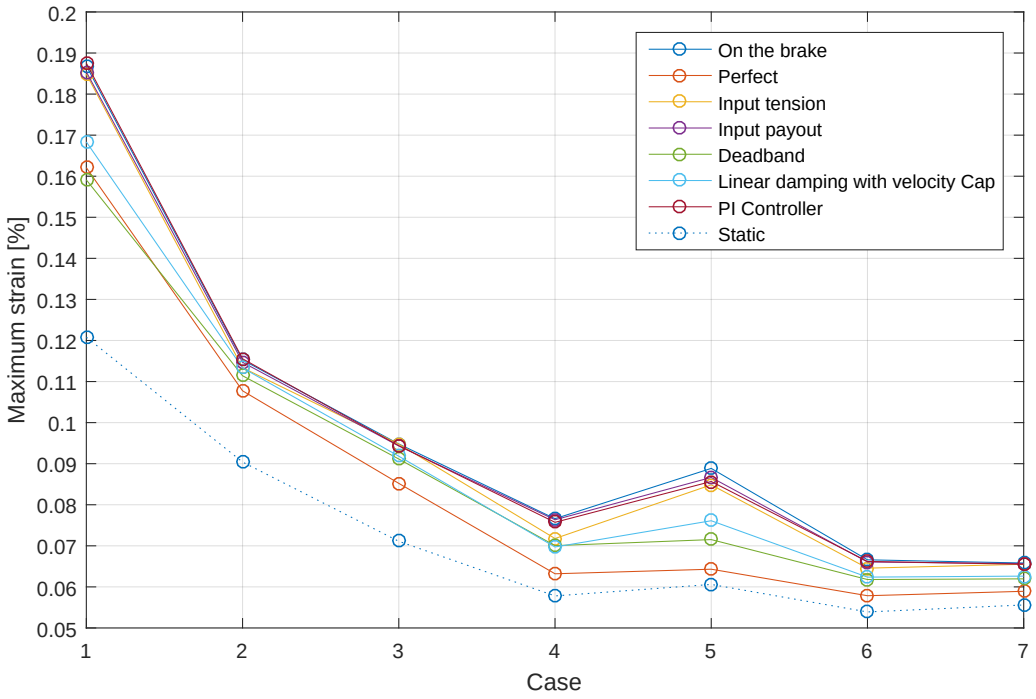

Figure 4.6: Summary of maximum von Mises strain

Table 4.3 shows the details of the data points in Figure 4.6.

Table 4.3: Summary of maximum von Mises strain

Case number	Maximum von Mises strain for each tensioner mode [%]						
	On the brake	Perfect	Input tension	Input payout	Deadband	Linear damping with velocity cap	PI Controller
1	0.187	0.162	0.185	0.185	0.159	0.168	0.188
2	0.115	0.108	0.113	0.115	0.111	0.113	0.116
3	0.095	0.085	0.095	0.094	0.091	0.092	0.094
4	0.077	0.063	0.072	0.076	0.070	0.070	0.076
5	0.089	0.064	0.085	0.087	0.072	0.076	0.086
6	0.067	0.058	0.065	0.066	0.062	0.062	0.066
7	0.066	0.059	0.066	0.066	0.062	0.063	0.066

It can be seen in Figure 4.6 that the maximum strain tends to be lower as the water depth increases. This is due to the maximum strain in static condition is becoming lower as water depth increasing. Therefore, it depends on the static configuration of the suspended pipeline.

Subsequently, the dynamic results are compared. Dynamic results are shown for several tensioner modes, with various compensation level. The tensioner on the brake is the mode where the tensioner does not compensate the tension fluctuation, and perfect tensioner is the mode where the tensioner completely compensates the tension fluctuation. The other tensioner modes are expected to be in between these two tensioner modes.

It is observed from the results of Case 1 to 7 that the perfect tensioner becomes more significant as the water depth increases. This can be attributed to the distance of the sagbend from the source of excitation, which is the vessel. The perfect tensioner keeps the tension constant at the top, but the bending moment propagation induced by the vessel motions is remaining. In deep water, the dynamic bending moment experienced by the sagbend is less due to the longer distance from the vessel compared to the shallow water case. While in shallow water, as the distance is shorter, the dynamic bending moment in the sagbend due to the vessel motions are larger.

Dynamic amplification is defined as the ratio of the maximum dynamic strain and the maximum static strain. As can be seen in Table 4.4, the largest dynamic amplification can be seen in Case 1. This is due to the vessel motions are the most severe among all cases. Subsequently, it is observed that the perfect tensioner and tensioner on the brake are the boundaries of the tensioner modes, except in Case 1 where the deadband model gives less strain than the perfect tensioner.

Table 4.4: Dynamic amplification of maximum von Mises strain

Case number	Dynamic amplificantion of max. von Mises strain						
	On the brake	Perfect	Input tension	Input payout	Deadband	Linear damping with velocity cap	PI Controller
1	1.55	1.34	1.53	1.53	1.32	1.39	1.55
2	1.28	1.19	1.25	1.27	1.23	1.25	1.28
3	1.33	1.20	1.33	1.33	1.28	1.29	1.33
4	1.33	1.09	1.24	1.32	1.21	1.21	1.31
5	1.47	1.06	1.40	1.43	1.18	1.26	1.41
6	1.24	1.07	1.20	1.23	1.15	1.16	1.23
7	1.18	1.06	1.18	1.18	1.11	1.13	1.18

Based on Table 4.4, it is observed that the active tension compensation becomes more important in deeper water as the reduction in maximum von Mises strain in the sagbend become more significant with increasing water depth. The maximum von Mises strain is found to be in between 0% and 2.2% lower from the model with tensioner on the brake.

As discussed in Section 2.4.4, the input payout mode which simulates the real tensioner behavior, hence the result from this tensioner mode is considered as the benchmark for the other tensioner models/modes.

The deadband and linear damping with velocity cap are observed to be not conservative as the maximum strain produced by models with these tensioner modes close to the model with a perfect tensioner. Moreover, the deadband model in shallow water (Case 1) gives a lower strain than the perfect tensioner model. Then, the input tension mode gives a close maximum strain to the input payout except in Case 4 and 6. Lastly, PI controller shows a good agreement with the input payout rate for all cases.

4.2.2. Fatigue Analysis

Figure 4.7 shows the allowable standby time for all cases with different tensioner models.

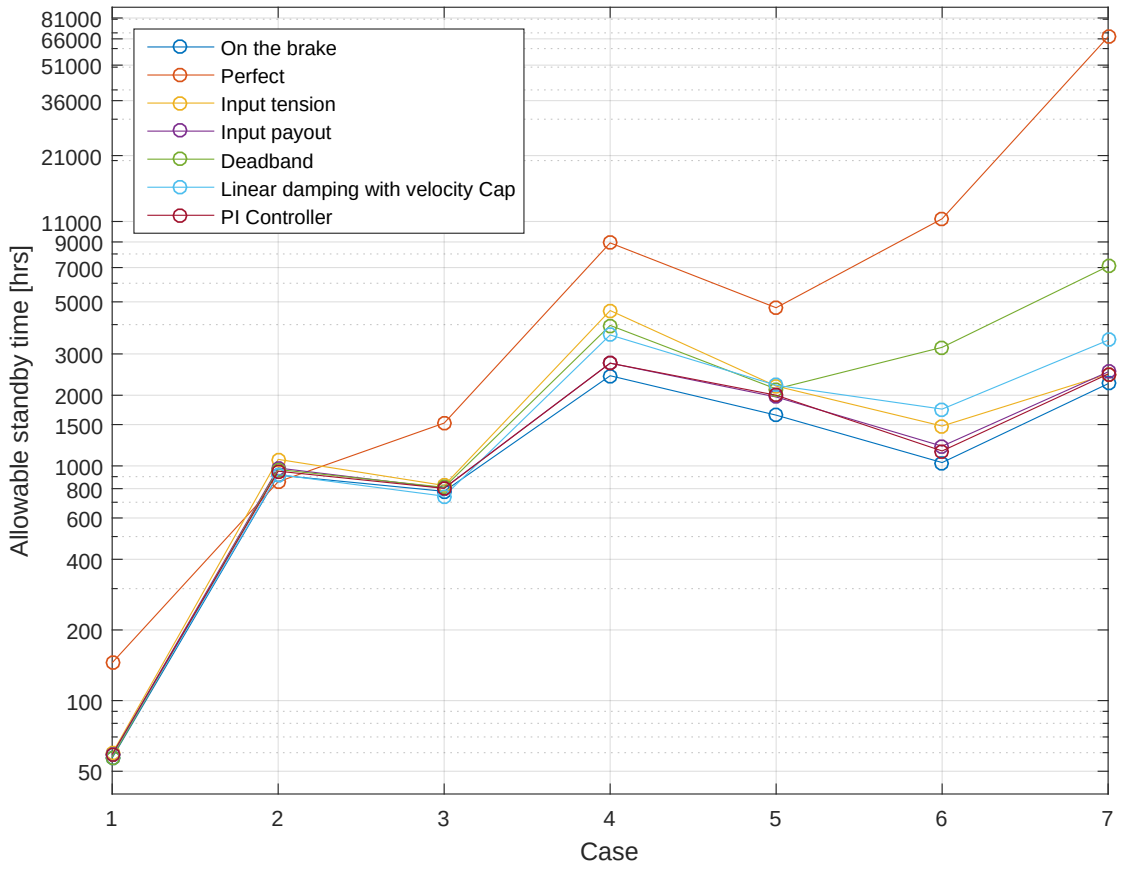

Figure 4.7: Summary of allowable standby time

The details of Figure 4.7 are shown in the Figure below,

Table 4.5: Summary of allowable standby time

Case number	Standby time for each tensioner mode [hrs]						
	On the brake	Perfect	Input tension	Input payout	Deadband	Linear damping with velocity cap	PI Controller
1	57	145	60	59	57	59	59
2	914	856	1066	979	965	919	949
3	779	1522	825	804	811	743	802
4	2422	8917	4592	2740	3969	3614	2740
5	1645	4719	2188	1966	2128	2206	2001
6	1033	11297	1479	1213	3201	1746	1158
7	2240	67344	2461	2515	7089	3431	2461

It can be seen that the allowable standby time generally increases as the water depth increases. This can be attributed to the geometry of the suspended pipeline. In shallow water, pipeline is more sensitive to vessel motions due to the relatively short length of the suspended pipeline thus a lighter mass. Therefore, the cyclic bending stress becomes more significant compared to deep water cases. A sharp increase in Case 4 is explained by the vessel motions since they are at the lowest among all cases. Subsequently, a decrease in

Case 6 is attributed to the lighter pipe section properties, which gives more dynamic effects compare to the heavier pipe as also explained by the sensitivity of concrete coating density in Section 3.2.2.

The deadband and linear damping with velocity cap models in shallow water show a similar results to the input payout mode. However, in deep water, it is not conservative as the standby time becomes extremely larger.

Despite the fact that perfect tensioner gives smaller maximum sagbend strain, the cumulated fatigue damage does not necessarily smaller. It can be seen in Case 2 where the perfect tensioner gives the shortest allowable standby time. This is evidently due to the damage rate at the worst node is larger for the perfect tensioner. Even though the accumulated fatigue damage at the pipe joint is smaller, due to this large damage rate at the worst node, the allowable installation time is shorter. This is attributed to the cyclic motions generated by the perfect tensioner.

In line with the maximum strain, accuracy of the PI controller model shows a good agreement with the input payout mode for all cases. Therefore, the PI controller model is valid and can be used for a more accurate investigation of the fatigue damage in all cases.

4.3. Chapter Conclusion

Dynamic amplification of the maximum von Mises strain is found to be significant in all water depth. The highest dynamic amplification found in Case 1 in the shallowest water. This is simply due to the vessel motions are at the largest compared to the other cases.

For predicting the maximum von Mises strain, deadband and linear damping with velocity cap models are not conservative as the maximum strains are closer to the perfect tensioner in all cases. While the input payout mode, which is the representation of reality, results in a maximum strain that is closer to the tensioner on the brake.

For the calculation of the accumulated fatigue damage, deadband and linear damping with velocity cap models are valid as the allowable standby time is similar to the input payout model. However, in deep water, these tensioner models are not conservative as the allowable standby time can be extremely large compared to the input payout model.

Despite the fact that a model with a perfect tensioner gives the smallest maximum von Mises strain, the accumulated fatigue damage is not guaranteed to be lower as well. It is found in Case 2 that the fatigue damages are larger due to the higher damage rate at the worst node. This is due to the cyclic loading induced by the perfect tensioner when maintaining the tension constant during simulation.

Damage rate at the worst node governs the allowable standby time as the lowest allowable standby time always corresponds to the model with tensioner modes with the highest damage rate at the worst node. In shallow water, it can be model with either tensioner on the brake, perfect tensioner, or deadband model. In deep water, it is likely to be the tensioner on the brake.

PI controller model shows a good agreement with the input payout rate model for both maximum von Mises strain and fatigue damage, in any installation cases. Besides the pipeline integrity, the tension fluctuation is also similar to the input payout model. This concludes that the tuning procedure given in Section 4.1.2 is valid. Among all tensioner models considered in this thesis, PI controller model is concluded as the most reliable controller model governing the tensioner behaviour for predicting pipeline integrity.

5

Conclusions and Recommendations

This thesis had focused on the significance of the active tension compensation on pipeline integrity during S-lay installation. In this final chapter, answers to the research questions are elaborated, the conclusion on what was achieved is summarized and recommendations for future work are given.

5.1. Conclusions

Deviation of the model output tension from the offshore measured tension is inevitable since a constant value added mass coefficient was used during the 3-hour simulation. While in reality, the added mass coefficient depends on the KC number, which means that the added mass coefficient change over time. The deviation is also caused by measurement sensors. The measurement signal is not exact due to the limited sampling rate of the load cells which measure the pipeline top tension.

The results of sensitivity analysis show that the uncertainty in the concrete coating weight might explain a large part of the tension overestimation by the model. This uncertainty in the pipeline weight can be attributed to the water absorption, material composition, and thickness of the concrete coating. In addition, Chapter 3 shows that the assumption of using the mean value of measured tension as set tension is not always valid. The mean value of the tension signal might be influenced by the presence of ocean current with significant velocity during offshore installation. Since a true match cannot be expected, the results found with tension peak relative deviations mostly lower than 10% are sufficient to validate the model.

Evaluating the drag coefficient at the maximum operating points and keeping it as a constant during the simulation has negligible effects on the results. On the other hand, the optimisation of the added mass coefficient is shown to have significant effects. Wave-induced force on the pipeline is found to be insignificant compared to the tension fluctuation induced by vessel motions. Therefore, the assumption of using the measured vessel motions as inputs to the model is valid. The effect of seabed model which is characterised by the undrained shear strength of the soil is negligible as the tension signal of these models are relatively the same. Therefore using the soil properties obtained from soil investigation at the closest investigation location is sufficient.

It is observed that the active tension compensation becomes more important in deeper water as the reduction in maximum von Mises strain in the sagbend and accumulated fatigue damage become more significant with increasing water depth. The maximum von Mises strain is found to be in between 0% and 2.2% lower from the model with uncompensated tension. Moreover, the reduction in accumulated fatigue damage is more significant as the allowable standby time increases between 3.2% and 19.5%.

The existing tensioner models which are currently used for pipelay analysis are not conservative as the maximum von Mises strain and accumulated fatigue damage are underestimated, with the exception of the accumulated fatigue damage in shallow water cases. As an alternative to the existing tensioner model, a tensioner model with a PI controller is introduced to represent the PI controller of the tensioners systems on the vessel. This PI controller model scripted in Python is implemented as an external function to the OrcaFlex model. Based on the pipeline integrity check, the tensioner model with PI controller is valid and can be used for a more accurate investigation of the pipeline integrity in all cases.

Lastly, the tensioner model with a PI controller can be used for a predictive study with specified Response Amplitude Operator (RAO) of the vessel and wave spectrum to simulate the wave load which generates vessel

motions. The PI controller computes the payout rate based on the pipeline top tension which is induced by the vessel motions. Therefore, the tensioner with PI controller model can be used for all types of vessel motions inputs.

5.2. Recommendations

Since the model is based on several fundamental assumptions, for instance, the set tension is assumed to be equal to the mean of the measured tension signal; thus there is room for improvement of the model presented in this thesis which will result in a more realistic model. Recommendation for future improvements is given based on the problem encountered during the attempt to answer the research question.

1. In order to validate the ocean current, it is recommended to measure the stinger tip clearance during offshore installation. Additionally, it is also recommended to do an experimental study which gives an accurate value of the submerged concrete coating weight.
2. Improvement in the sampling rate of the payout measurement is needed to simulate a more accurate tensioner behaviour. An acceleration sensor is expected to give a more accurate measurement result.
3. It is highly recommended to choose the time frame of the case studies within the period without pulls.
4. It is recommended to study all the possible controller gains of the PI controller on the vessel. Based on this, the range of controller gains for the PI controller model can be achieved, and recommendation of controller settings that can be used for a predictive study can be given.

A

Appendix

A.1. Measurement Data Amplitude Spectrum

A.1.1. Vessel motions

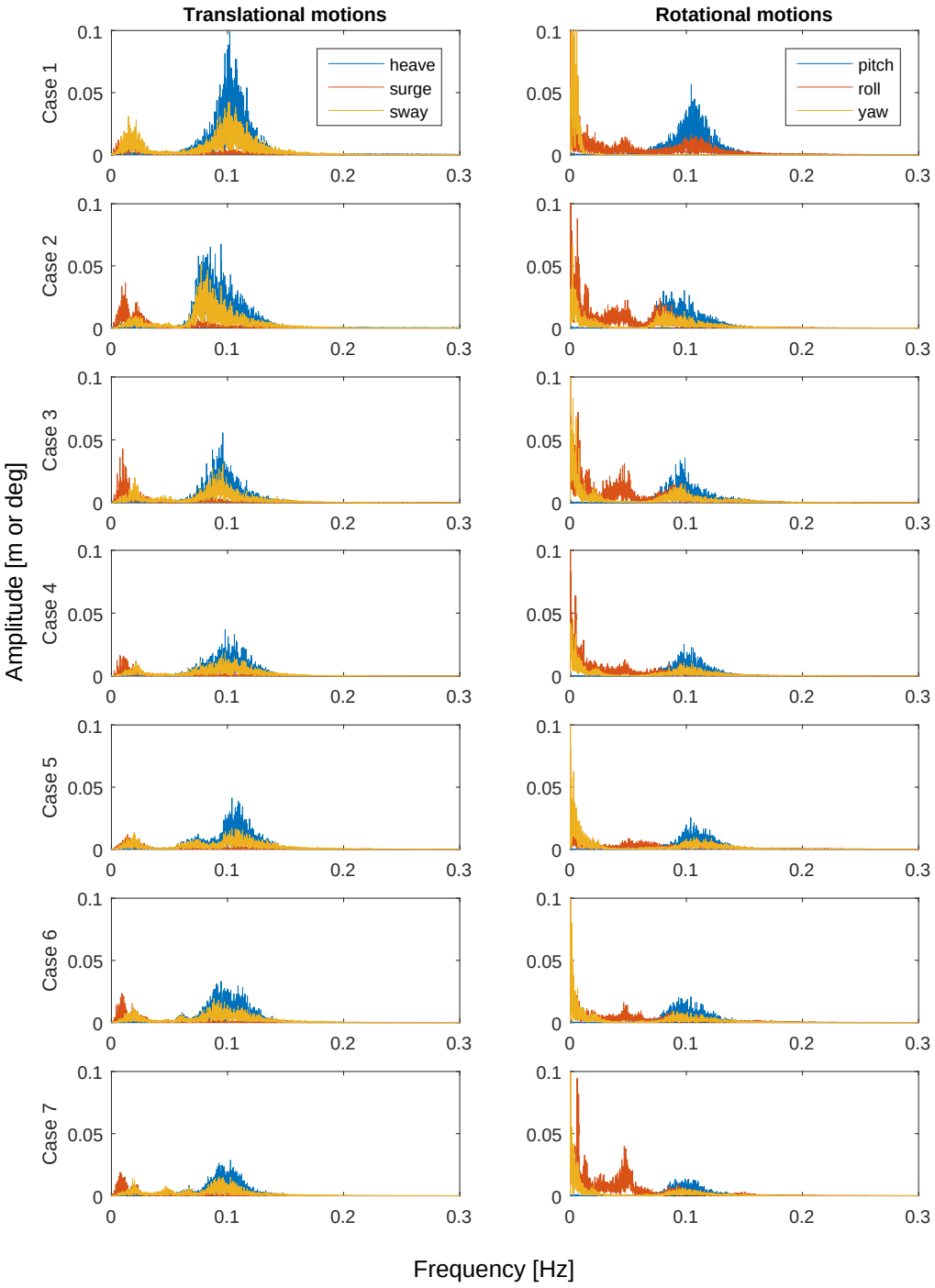

Figure A.1: Amplitude spectrum of vessel motions

A.1.2. Payout rate

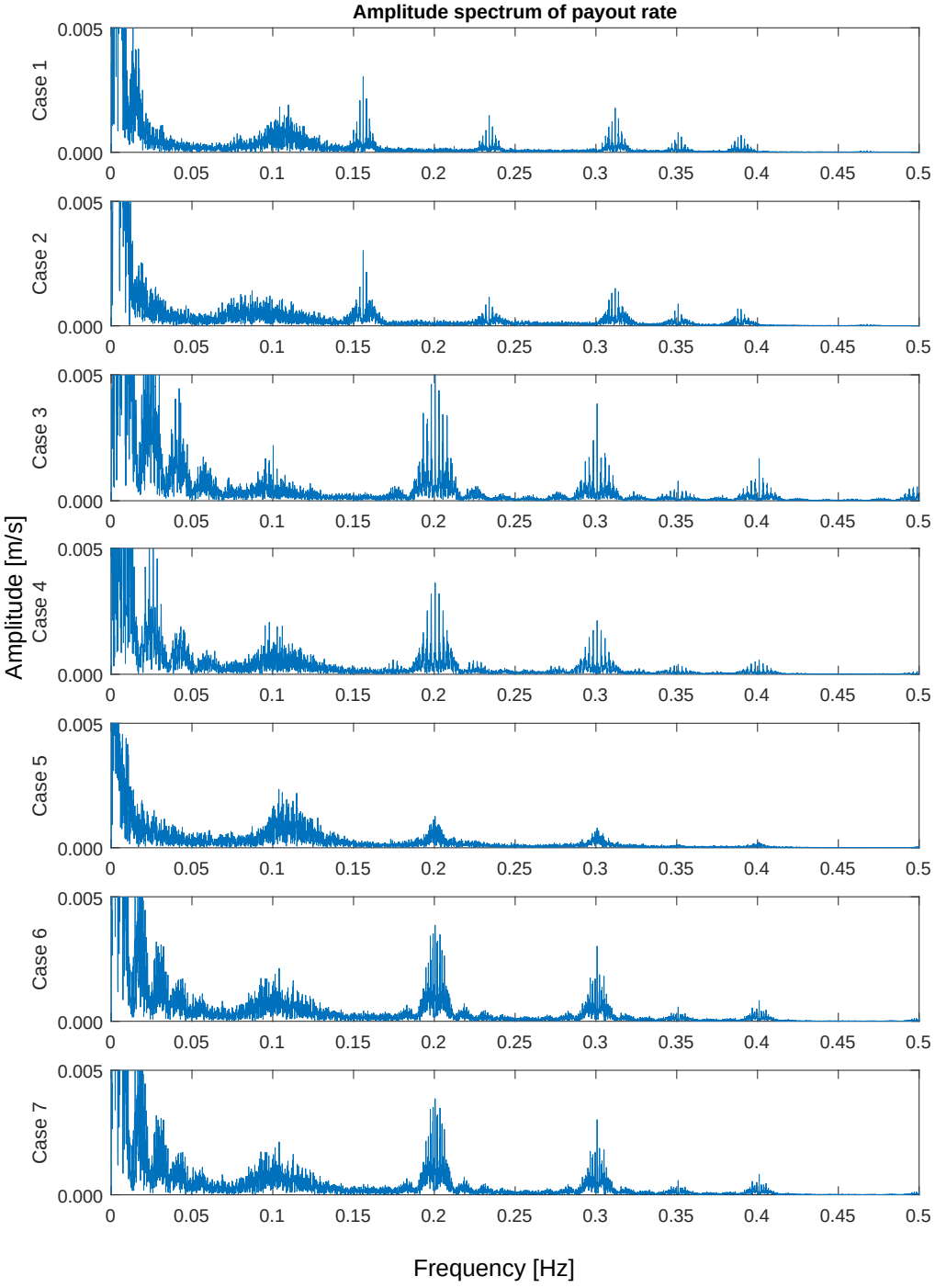

Figure A.2: Amplitude spectrum of tensioner payout rate

A.1.3. Pipeline top tension

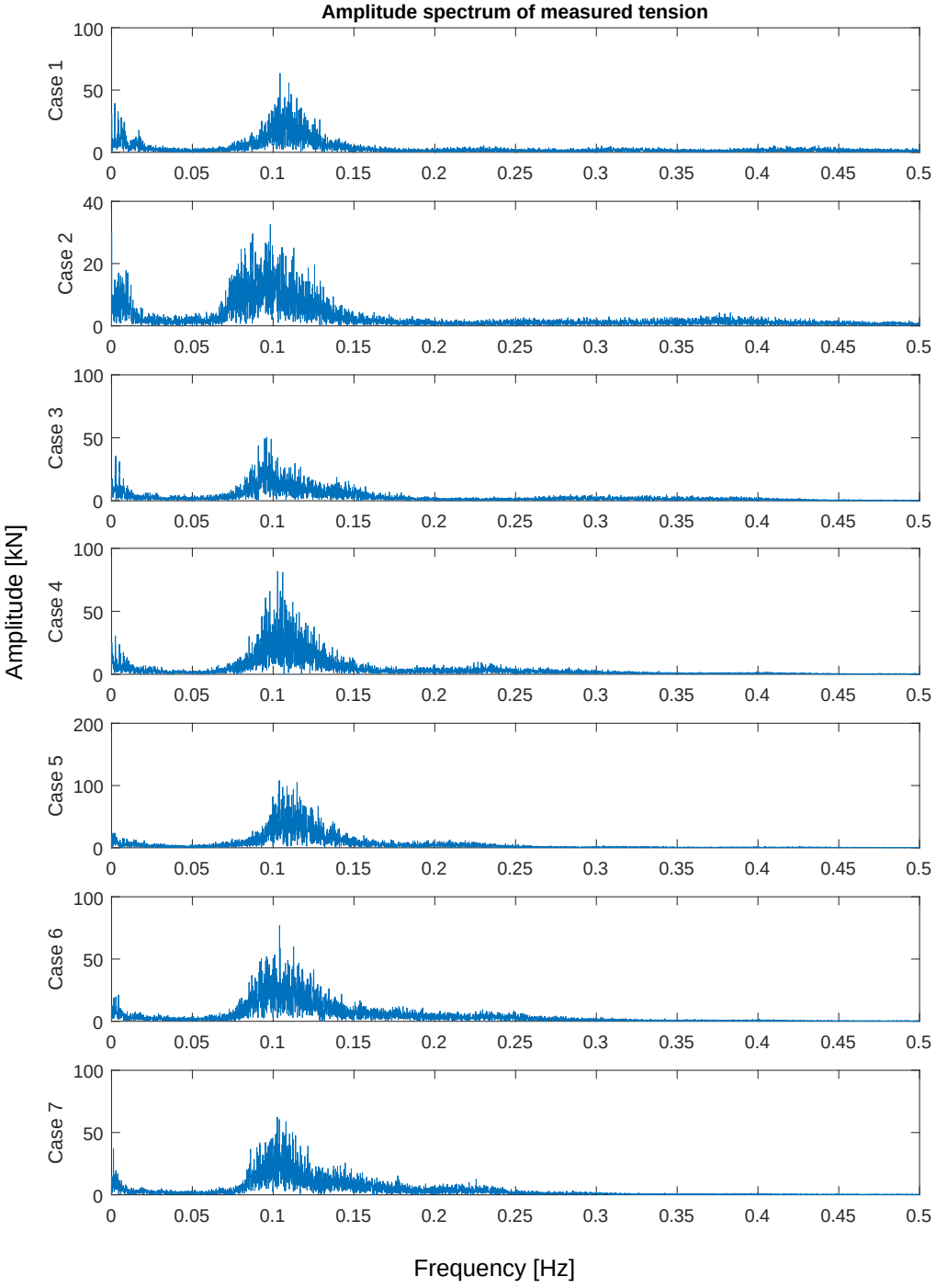

Figure A.3: Amplitude spectrum of pipeline top tension

A.2. Range Graph of KC Number

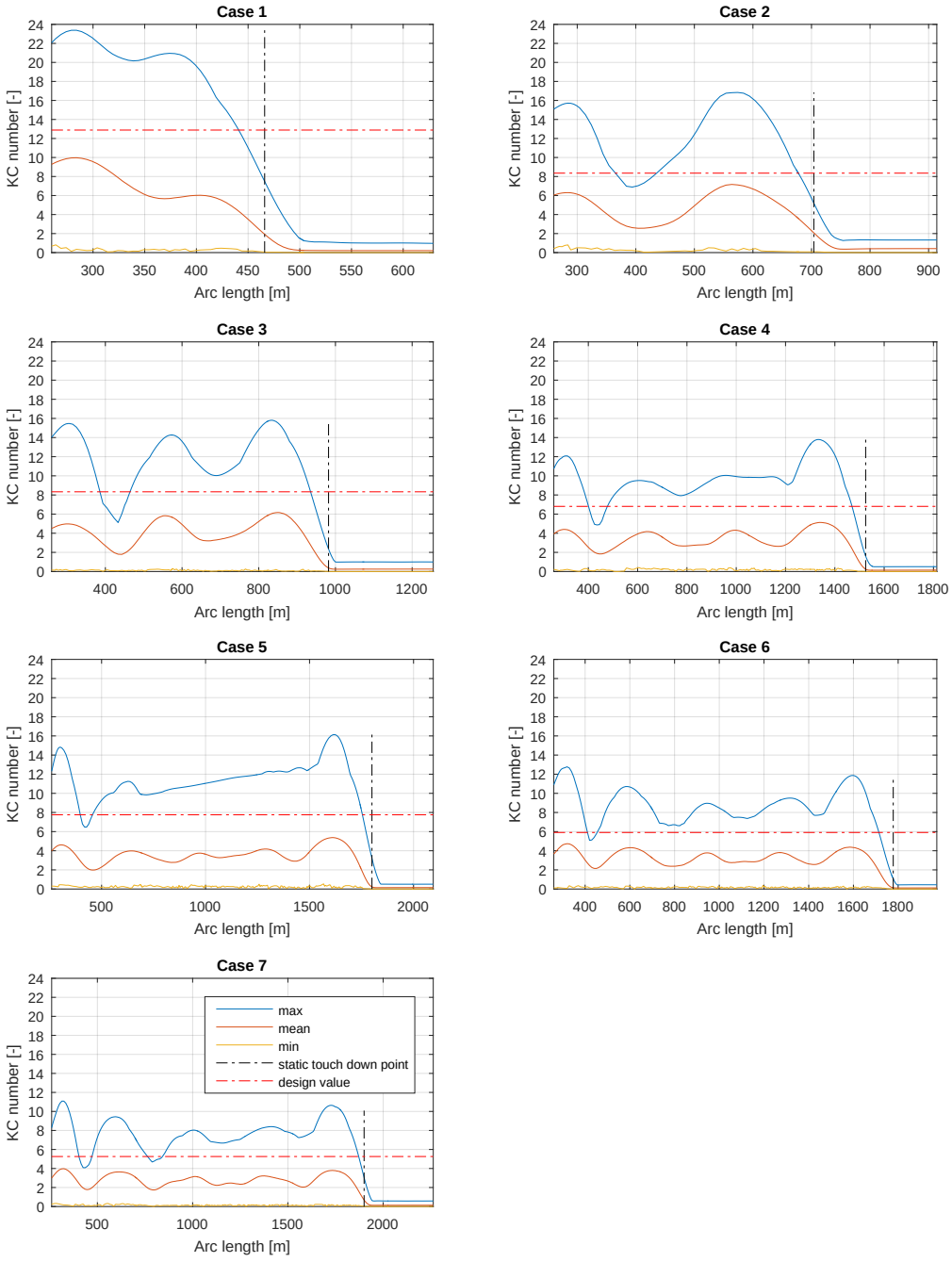

Figure A.4: Overview of Keulegan-Carpenter number

A.3. Sensitivity Analysis Results for Concrete Coating Density

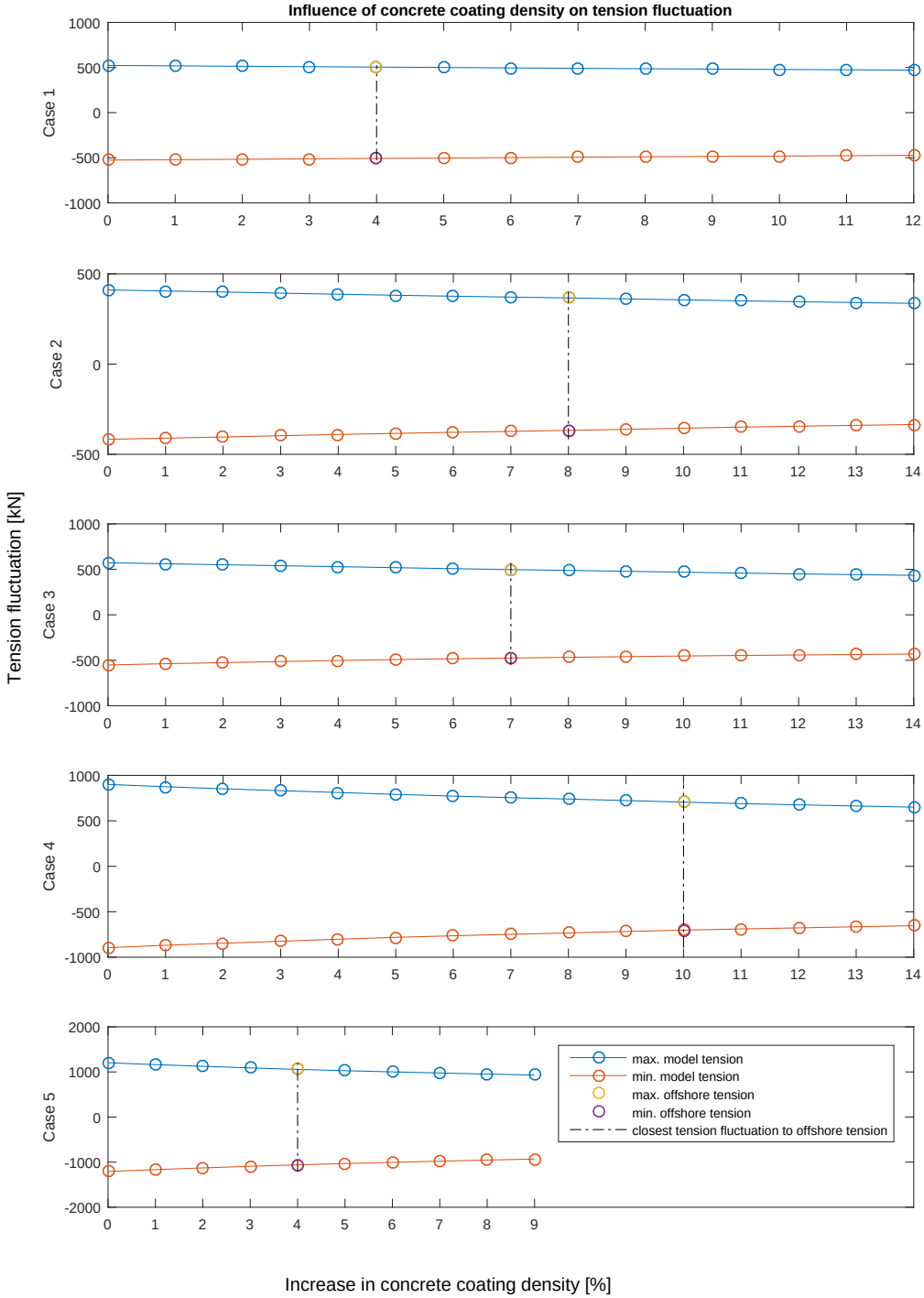

Figure A.5: Overview of concrete coating sensitivity analysis results

A.4. Python Script of the PI Controller Model

```
"""
Created on Thu Mar 23 11:52:26 2017

@author: TSj

This module is an external function of PID Controller for use with OrcaFlex to
calculate payout rate of the tensioners.

"""
import json

class PIDstate(object):
    def __init__(self):
        self.valid = False
        self.time = -OrcFxAPI.OrcinaInfinity()
        self.signal = 0.0
        self.iedt = 0.0
        self.dedt = 0.0

    def getStateAttributes(self):
        return {
            'valid': self.valid,
            'time': self.time,
            'signal': self.signal,
            'iedt': self.iedt,
            'dedt': self.dedt,
        }

    def setStateAttributes(self, attributes):
        self.valid = attributes['valid']
        self.time = attributes['time']
        self.signal = attributes['signal']
        self.iedt = attributes['iedt']
        self.dedt = attributes['dedt']

class PIDController(object):

    def Initialise(self, info):

        self.periodNow = OrcFxAPI.Period(OrcFxAPI.pnInstantaneousValue)

        params = info.ObjectParameters
        def GetParameter(paramName, default=None):
            if paramName in params:
                param = params[paramName]
                if isinstance(default, float):
                    param = float(param)
                elif isinstance(default, int):
                    param = int(param)
            elif not default is None:
                param = default
            else:
                raise Exception('Parameter %s is required but is not included \
                in the object parameters.' % paramName)
```

```
        return param

    self.timedata = GetParameter('time')
    self.P = GetParameter('P_gains')
    self.I = GetParameter('I_gains')
    self.D = GetParameter('D_gains')

    self.timedata = [float(i) for i in \
    self.timedata.strip('{}').split(',')]

    self.P = [float(i) for i in self.P.strip('{}').split(',')]
    self.I = [float(i) for i in self.I.strip('{}').split(',')]
    self.D = [float(i) for i in self.D.strip('{}').split(',')]

    self.ControlledObject = info.Model[GetParameter('ControlledObject')]
    self.ControlStartTime = GetParameter('ControlStartTime',\
    -OrcFxAPI.OrcinaInfinity())
    self.TargetValue = GetParameter('settension', 0.0)
    self.nodenumber = int(GetParameter('nodenumber', 0.0))
    self.ObjectExtra = OrcFxAPI.oeNodeNum(self.nodenumber)

    self.MinValue = GetParameter('MinValue', -OrcFxAPI.OrcinaInfinity())
    self.MaxValue = GetParameter('MaxValue', OrcFxAPI.OrcinaInfinity())

    # If info.StateData is not None then we have been called when loading
    # a simulation, so we need to restore the controller state
    # to what our StoreState() method saved when the simulation was stored:
    self.prev = PIDstate()
    self.now = PIDstate()

    if info.StateData:
        import json
        state = json.loads(info.StateData)
        self.now.setStateAttributes(state['now'])
        self.prev.setStateAttributes(state['prev'])
    else:
        # This is a new simulation, so initialise the controller state:
        self.prev.iedt = GetParameter('Initial e/D', 0.0)
        self.now.dedt = GetParameter('Initial De', 0.0)

    print('Initialised OK.')


def Calculate(self, info):

    if info.SimulationTime < self.ControlStartTime:
        return


    # If this is a new time step, and not the first, then step self.now
    # back to become our new self.prev:
    if info.NewTimeStep and self.now.valid:
        self.prev.time = self.now.time
        self.prev.signal = self.now.signal
        self.prev.iedt = self.now.iedt
        self.prev.dedt = self.now.dedt
```

```
            self.prev.valid = True
#            print('t=',self.now.time)

        # Get the state values now:
        self.now.time = info.SimulationTime
        self.now.signal = self.ControlledObject.TimeHistory\
        ('Effective Tension',self.periodNow,self.ObjectExtra)[0] # TimeHistory
        #returns an array, which in this case contains just 1 item, the value
        #now

        self.now.iedt = self.prev.iedt
        self.now.valid = True


        e = self.TargetValue - self.now.signal
        if self.prev.valid:
            prev_e = self.TargetValue - self.prev.signal
            dt = self.now.time - self.prev.time;
            self.now.dedt = (e-prev_e)/dt;
            self.now.iedt += dt*(e+prev_e)/2.0;

        self.idx = next(x[0] for x in enumerate(self.timedata) if x[1] > \
        info.SimulationTime) - 1
#
        self.kP = self.P[self.idx]
        self.kI = self.I[self.idx]
        self.kD = self.D[self.idx]

        info.Value = self.kP*e + self.kI*self.now.iedt + self.kD*self.now.dedt

#       Keep the tensioner speed within the specified limits:
        info.Value = max(self.MinValue, min(info.Value, self.MaxValue))


    def StoreState(self, info):

        import json
        state = {'now': self.now.getStateAttributes(), 'prev': \
        self.prev.getStateAttributes()}
        info.StateData = json.dumps(state)
```

Bibliography

[1] OrcaFlex documentation,
https://www.orcina.com/SoftwareProducts/OrcaFlex/Documentation/Help/

[2] Morison, J. R.; O'Brien, M. P.; Johnson, J. W.; Schaaf, S. A., *The force exerted by surface waves on piles.* Petroleum Transactions, American Institute of Mining Engineers.

[3] DNV-RP–C205, *Environmental conditions and environmental loads.* Norway: Recommended Practice, DNV. (2007).

[4] Matsuishi, M. and Endo, T., *Fatigue of metals subjected to varying stress.* Japan Soc. Mech. Engineering.

[5] Maddox S. J., *Fatigue strength of welded structures.*Woodhead Publishing Ltd, ISBN 1 85573 013 8.

[6] Rychlik I., *A new definition of the rainflow cycle counting method.*Int. J. Fatigue 9, No 2, 119-121.

[7] Anders Brandt, *Noise and Vibration Analysis: Signal Analysis and Experimental Procedures.*John Wiley & Sons, Ltd.

[8] Karl Johan Astrom and Richard M Murray, *Feedback Systems: An Introduction for Scientists and Engineers.*Princeton University Press.

[9] Randolph M. and Quiggin P., *Nonlinear hysteretic seabed model for catenary pipeline contact.*OMAE paper 79259, 2009.

[10] Randolph M. and White, *Pipeline embedment in deep water: processes and quantitative assessment.*Proc. Offshore Technology Conf., Houston, Paper OTC 19128.

[11] Polarled pipeline project, *Geotechnical design for Prelay Span Supports.* Detailed Engineering Design, Doc. number: D142-RM-P300-F-RD-034.

[12] Chung J. and Hulbert G. M., *A time integration algorithm for structural dynamics with improved numerical dissipation: The generalized-α method.*ASME Journal of Applied Mechanics. 60, 371-375.

[13] MathWorks, *Matlab Documentation: R2017b.* Retrieved November 30, 2017 from https://nl.mathworks.com/help/.